nature biomedical engineering

SUPPLEMENTARY INFORMATION

https://doi.org/10.1038/s41551-019-0462-8

In the format provided by the authors and unedited.

Functionalized helical fibre bundles of carbon nanotubes as electrochemical sensors for long-term in vivo monitoring of multiple disease biomarkers

Liyuan Wang[1,4], Songlin Xie[1,4], Zhiyuan Wang[2,4], Fei Liu[3], Yifan Yang[3], Chengqiang Tang[1], Xiaoying Wu[1], Peng Liu[1], Yongjing Li[1], Hexige Saiyin[2], Shuang Zheng[1], Xuemei Sun[1*], Fan Xu[3*], Hongbo Yu[2*] and Huisheng Peng[1*]

[1]State Key Laboratory of Molecular Engineering of Polymers, Department of Macromolecular Science and Laboratory of Advanced Materials, Fudan University, Shanghai, China. [2]Vision Research Laboratory, School of Life Sciences, State Key Laboratory of Medical Neurobiology, Collaborative Innovation Centre for Brain Science, Fudan University, Shanghai, China. [3]Department of Aeronautics and Astronautics, Fudan University, Shanghai, China. [4]These authors contributed equally: Liyuan Wang, Songlin Xie, Zhiyuan Wang. *e-mail: sunxm@fudan.edu.cn; fanxu@fudan.edu.cn; hongboyu@fudan.edu.cn; penghs@fudan.edu.cn

Supplementary Notes:

Materials and Methods

1. Preparation of single-ply and multi-ply sensing fibres

1.1 Preparation of CNT fibres

1.1.1 Typical chemical vapour deposition

The CNT arrays were synthesized *via* chemical vapour deposition with Fe (1 nm)/Al_2O_3 (10 nm) as the catalyst on a silicon substrate, and flowing ethylene (90 sccm), Ar (400 sccm) and H_2 (30 sccm) as carbon source, carrier gas and reduction gas, respectively[1]. The synthesis occurred continuously at the hot zone of a tube furnace with the reaction temperature of 740 °C for 10 min. CNT sheets with a thickness of ~250 nm and a width of ~1 cm were dry drawn from the array, and further twisted to produce the CNT fibres (typical diameter of 16 μm) **(Figure 1b–d)**. The diameter of CNT fibre could be controlled from 1 to 50 μm by the width and layer number of CNT sheets.

1.1.2 Floating chemical vapour deposition

The CNT fibres were synthesized *via* floating catalyst chemical vapour deposition with thiophene (1-2 wt%) and ferrocene (1-2 wt%) as the catalyst, and flowing ethanol (> 97 wt%), Ar (200 sccm) and H_2 (2000 sccm) as carbon source, carrier gas and reduction gas, respectively[1]. CNT aerogel was produced continuously at the hot zone of a tube furnace with the reaction temperature of 1200 °C, and it was then collected into cylindrical hollow socks. The CNT sock was pulled out of the furnace by a titanium rod and then densified through water and ethanol in turn. The CNT sock shrank immediately into CNT ribbon upon arriving at the water surface. It was finally washed by acetone for further densification, followed by drying, twisting and collecting onto a spool to produce the CNT fibres (typical diameter of 50 μm) (**Figure S1**). The diameter of CNT fibre could be controlled from 10 to 200 μm. Unless otherwise specified, the CNT fibre in this project was prepared by floating chemical vapour deposition.

1.2 Fabrication of single-ply sensing fibres (SSFs)

1.2.1 Preparation of H_2O_2 SSFs

The H_2O_2 SSF was prepared by depositing Pt nanoparticles into CNT fibre through an electrochemical double potential step method. KCl (0.1 M, Sinopharm) and K_2PtCl_6 (1 mM, Sigma) aqueous solution was used as the electrolyte, and CNT fibre, Pt wire (Shanghai Yueci), Ag/AgCl (Shanghai Yueci) were used as working, counter and reference electrodes,

respectively. In a typical electrochemical cycle, the deposition was conducted by setting the first step at 0.5 V for 10 s and the second step at –0.7 V for 10 s. The Pt/CNT composite fibre was obtained after 50 cycles.

1.2.2 Fabrication of glucose SSFs

Multi-step electrochemical procedure was used to fabricate glucose SSFs[2]. For enzyme-based glucose SSF, Firstly, PANI was deposited as an electron transport layer to widen the linear range by chronoamperometry method at 0.75 V for 20 s in the aqueous electrolyte consisted of 0.5 M aniline (Sinopharm) and 1 M H_2SO_4 (Sinopharm), with Pt wire and Ag/AgCl as counter and reference electrodes, respectively. Secondly, Pt nanoparticles were deposited onto the PANI/CNT fibre by using the same method as described in **1.2.1**. Thirdly, glucose-responsive layer was coated. Chitosan (Aladdin) solution of 1 wt% was prepared by dissolving chitosan in 2 wt% acetic acid (Sinopharm) aqueous solution under magnetic stirring for about 1 h, and it was then mixed with SWCNTs (2 mg mL^{-1}, Aladdin) under ultrasonic agitation. Glucose oxidase (40 mg mL^{-1}, Aladdin, GOx) was added to chitosan/SWCNTs solution. The mixed solution (4 μL) was dipped onto the Pt/PANI/CNT fibre with a length of 500 μm. After drying at the room temperature, Nafion aqueous solution (2 μL, 0.5 wt%, Sigma) was dip-coated onto the GOx/Pt/PANI/CNT fibre. Finally, the working electrode was immersed into glutaraldehyde (2 wt%, Aladdin) aqueous solution for 30 min. Nafion film was crosslinked by glutaraldehyde to form micropores, which could enhance selectivity and broaden the linear range. The glucose SSFs were obtained after drying overnight at 4 °C in the dark. The solutions and SSFs were stored at 4 °C.

For ZnO-based glucose SSF[3], ZnO nanoparticles (Aladdin, 0.24 g) and MWCNT-COOH (Sigma, 0.08 g) were dissolved in a mixture of 10 mL water and 15 mL ethylene glycol, dispersed by ultrasonic treatment and stirred for 20 h at 80 ^{o}C. The resulting product was washed with water and ethanol and dried at 60 ^{o}C. To make a glucose-sensing fibre, 0.05 g of ZnO/MWCNT was dispersed in a small amount of DMF and mixed with 5% Nafion aqueous solution (3/1, v/v) *via* stirring for 24 h. The mixture (3 μL) was dipped onto the CNT fibre, and a ZnO-based glucose SSF was obtained after drying at 50 °C.

1.2.3 Fabrication of SSFs for ions

For Ca^{2+} SSFs, poly(3,4-ethylenedioxythiophene)-poly(styrenesulfonate) (PEDOT:PSS) and Ca^{2+} selective membrane cocktail were coated onto the CNT fibre to prepare Ca^{2+} SSFs. Firstly, PEDOT:PSS aqueous solution (Heraeus, Al4083) was coated on the CNT fibre for

three times. Secondly, calcium ionophore □ (1% by weight, w/w, Sigma), sodium tetraphenylborate (0.55% w/w, Sigma), polyvinyl chloride (33% w/w, Sigma), and bis (2-ethylehexyl) sebacate (65.45% w/w, Aladdin) were mixed to prepare Ca^{2+} cocktail. Thirdly, 100 mg of the membrane cocktail was dissolved in 660 μL of tetrahydrofuran (Aladdin). PEDOT:PSS/CNT fibre was dipped into the solution and uniform coating was obtained. The Ca^{2+} SSFs were last allowed to dry overnight at 4 °C in the dark. All the solutions were stored at 4 °C.

For Na^+ SSFs[4], the Na^+ membrane cocktail was prepared by mixing Na ionophore X (1% by weight, w/w, Sigma), Na-TFPB (0.55% w/w, Sigma), polyvinyl chloride (33% w/w, Sigma), and bis (2-ethylehexyl) sebacate (65.45% w/w, Aladdin). Then 100 mg of the Na^+ membrane cocktail was dissolved in 660 μL of tetrahydrofuran (Aladdin). For K^+ SSFs, the K^+ membrane cocktail was a mixture of valinomycin (2% by weight, w/w, Sigma), NaTPB (0.5% w/w, Sigma), polyvinyl chloride (32.7% w/w, Sigma), and bis (2-ethylehexyl) sebacate (64.7% w/w, Aladdin). Then 100 mg of the K^+ membrane cocktail was dissolved in 350 μL of cyclohexanone (Aladdin). The other steps were the same as Ca^{2+} SSFs.

For pH SSFs, 0.1 M aniline/0.1 M H_2SO_4 solution was prepared and the pH SSFs was fabricated in the mixed solution by cyclic voltammetry from −0.2 to 1 V for 25 cycles at 100 mV/s.

1.2.4 Fabrication of prostate specific antigen (PSA) SSFs

A simple amperometric peptide-based PSA SSF was developed. The fabrications were summarized below43. Firstly, Poly(diallyldimethylammonium chloride) (PDDA)-GO solution was obtained as follows: graphene oxide (GO) aqueous solution (0.5 g/L) was obtained by magnetic stirring for about 6 h. PDDA (114 μL, 35%, w/w, Sigma) aqueous solution, 1.169 g NaCl (Sinopharm) and GO aqueous solution (20 mL, 0.5 g/L) were mixed, centrifuged and dissolved in 10 mL water. Secondly, chitosan solution (0.1 wt%) was prepared and mixed with K4[Fe(CN)6] (10 μL, 0.5 wt%, Sinopharm) aqueous solution, 60 μL PDDA-GO solution and 1.120 mL water. Thirdly, CNT fibre was dipped in the mixture every 3 min for 20 times. After drying, glutaraldehyde (0.05 wt%) was mixed with Pb(NO3)2 (0.1 M, Aladdin), and the fibre was immersed into the mixture for 30 min, followed by washing with water for twice. After that, the above modified fibre was immersed with 1 wt% glutaraldehyde for 30 min, washed with water for three times. Finally, peptide (0.2 mg mL-1, Solarbio) was mixed with albumin from bovine serum (0.01 mg mL-1, Sigma) aqueous solution. The fibre was

immersed into the mixture for 1 h. The PSA-SSFs were obtained after drying overnight at 4 °C in the dark.

1.2.5 Fabrication of the reference electrode

The Ag/AgCl reference electrode was prepared by cyclic voltammetry method. Firstly, the CNT fibre was immersed into a mixed aqueous solution consisted of 5 mM $AgNO_3$ and 1 M KNO_3 by sweeping from –0.9 to 0.9 V for 7 cycles at a scan rate of 0.1 V s^{-1}, with a two-electrode system where CNT fibre acted as working electrode and a commercial silver electrode (Shanghai Yueci) served as both the counter and reference electrode. Secondly, the Ag/CNT fibre was dipped in an aqueous solution of 0.1 M KCl and 0.01 M HCl by sweeping from -0.15 to 1.05 V for 2 cycles at a scan rate of 0.05 Vs^{-1} with a commercial Ag/AgCl as both the counter and reference electrode. The Ag/AgCl reference fibre electrode was obtained after drying. The Ag/AgCl reference fibre electrode was coated with a polymer layer based on Nafion/glutaraldehyde aqueous solution before implanted. The other reference electrodes, such as solid state reference electrode based on polymers, may be also introduced in the future[6].

1.3 Fabrication of multi-ply sensing fibre (MSF)

1.3.1 MSF for spatial analysis

The structure of MSF for spatial analysis was demonstrated with the Ag/AgCl fibre electrode as a core and five H_2O_2 SSFs being uniformly arranged along axial direction (**Figure 3e**). The fabrications are summarized below[7]. Firstly, every individual H_2O_2 SSF was fabricated as **1.2.1**, and PDMS as the insulating layer was dipped on the SSFs and solidified at 80 °C for 30 min. Secondly, all the H_2O_2 SSFs were arranged in parallel with space of 50 μm. The end of H_2O_2 SSFs was cut into a wedge with an angle of θ from the reference electrode. The magnitude of the angle depended on the size of the end gradient. Finally, one end was fixed by a rotating motor shaft and the other was fixed by adhesive tape. The motor was operated at a speed of 200 rad/min.

1.3.2 MSF for multiplex monitoring

The structure of the MSF for multiplex monitoring was similar to the MSF for spatial analysis, with the Ag/AgCl fibre electrode as a core and five different SSFs being uniformly arranged around the core (**Figure 3f**). In this work, pH, K^+, Na^+, Ca^{2+} and glucose SSFs were chosen as the model for the test in a mixed solution, and Ca^{2+} and glucose SSFs were chosen for the test *in vivo*. The fabrication typically included three steps. Firstly, all SSFs were prepared as **1.2.2**

and 1.2.3., and PDMS as insulating layers was dipped on the SSFs and solidified at 80 °C for 30 min. Secondly, all the SSFs were arranged in parallel with space of 50 μm, and the ends of SSFs were arranged with an angle of θ from the reference electrode. Finally, one end was fixed by a rotating motor shaft and the other was fixed by adhesive tape. The motor was operated at a speed of 200 rad/min.

2. Injection of the sensing fibres

2.1 Animal preparation

The experiment protocols were approved by Animal Experimentation Committee of Fudan University. All animals were treated in accordance with guidelines for the care and use of experimental animals described by the National Institutes of Health and Fudan University.

Ten adult cats (female, about 1.5–2.5 kg in weight) and three adult cats (male, about 1.5–2.5 kg in weight) were purchased from Shanghai Yingen Farm. Seven weeks BALB/c nude mice (female, about 20 g in weight) were purchased from Shanghai SLAC Laboratory animal CO. Ltd. To develop the tumour model, 1×10^7 /0.2 mL A549 cancer cells in phosphate buffer saline (PBS) solution were injected into the armpit of each mouse. Weight of the mice and tumour size (Volume = (length × width^2)/2) were recorded every two days.

2.2 The loading and injection methods of the SSF with a syringe

The sensing fibre was thread into the 1-mL-syringe pre-filled with normal saline[8]. Sensing terminal of the fibre was kept in needle and the other parts were left in syringe body. The speed of injection was about 1.0 mm s^{-1} for intravenous injection and subcutaneous injection.

2.3 Intravenous injection

Cats were kept anesthetized during experiment, given with 5% isoflurane at an air flow rate of 1000 cc/min for anesthesia induction and 2.5% isoflurane at an air flow rate of 800 cc/min for anesthesia. The hair over the femoral vein was removed by depilatory cream and the skin was cleaned by iodophor and 75% (v/v) alcohol. Then the fibre was injected into the femoral vein by intravenous injection (**Figure 1f**) along with the solution flowing. After injection, the needle was retreated from the vein, bleeding was stanched by compression of a swab, and silver paint was covered outside individual SSF.

2.4 Subcutaneous tumour tissue injection

Mice were kept anesthetized during experiment, given with 1% isoflurane at an air flow rate

of 300 cc/min for anesthesia. Then the MSF for spatial analysis was injected into a tumour tissue (with diameter of 1.0 to 1.5 cm) near the forelimb from the anesthetized mouse by intramuscular injection for spatial analysis. After injection, the needle was withdrawn from the tumour tissue and conductive silver paint was coated on the end of each SSF.

2.5 Evaluation of injection method: wound caused by device injection and elimination

The operating room was sterilized by ultraviolet light for 30 min before the surgery, and all surgical instruments were sterilized by dry heating to 150 °C for 3 h, so the surgery could be taken under aseptic condition. Cat was anesthetized and the hair near the femoral vein was removed as described in **Supplementary 2.3**.

The CNT fibre was injected as described in **Supplementary 2.3**. The wound containing the fibre was observed by a stereoscopic microscope (**Figure 1g** and **Figure S3a**). After sticking the fibre, the animal was awakened and returned into the cage for the following observation. The wound was observed for over 4 d to estimate the chronic inflammation (**Figure S4**). The other fibre was injected as the same way and was pulled out after 30 min. The wound was then observed by a stereoscopic microscope. The observation was made at 2, 4, 6, 24 and 48 h after the injection (**Figure S6**).

As for the control group, an incision around 1.5 cm was cut by a scalpel to implant a PDMS film with around 2 cm long, 5 mm wide and ~100 μm thick (**Figure S3b**). Wound was observed for over 4 d. After observation, the wound was sutured by surgical cotton fibre suture and the film was stitched tightly on the tissue. Sulfanilamide was sprinkled on the wound and iodophor was swabbed on the incision wound every two days.

3. Implants prepared for mechanical and biocompatibility study

3.1 The preparation of the implants

Gold wires with diameters of ~50 μm were obtained from Alfa.

3.2 The implanting method

Cats were anesthetized and the hair on the leg was removed. Gold wires were injected into the bare skin on the leg of the cat as described in **Supplementary 2.2**, which was similar to the injection method of CNT fibre.

3.3 Cell Counting Kit-8 (CCK-8) and Live or Death^{TM} cell viability test

CNT films were cut down into small sizes by about 5 mm × 5 mm and were placed into a 24-well plate after sterilization. For cell cultivation, 0.5 mL suspended L929 cells (4×10^4 cell/mL, Shanghai R&S Biotechnology Co. Ltd.) were seeded into two 24-well plates, one with CNT films and the other with glass as a control group and were cultivated under 37 ^oC and 5% CO_2. Both groups were cultivated in the same way and taken for CCK-8 test (CK04, dojindo) after cultivating for 1, 3, 5, 7 d separately. For CCK-8 test, 10 μL CCK-8 was added to each well. The OD450 of both treated cell and blank was measured by microplate spectrophotometer (Thermo, MuLTiSKAN MK3) after incubating for 2 hours. To minimize the error caused by serum, OD450 of treated cell should subtract OD450 of blank. The CCK-8 test was repeated for 9 times.

CNT and control group of L929 cells were taken for Live or Death™ cell viability test (22788, AAT Bio Inc.) after cultivated for 3 and 5 days. For Live or Death™ cell viability test, the dye-loading solution was prepared by adding 5 μL of 200X Cellbrite™ Red and 5 μL of 200X Nuclear Blue™ DCS1 to 1 mL of Assay Buffer. To ensure validity, the solution should be used in 1 h at room temperature. Cell growth medium was replaced with 1 mL dye-loading solution. After incubated at 37 ^oC for 45 min without contacting light, cells were washed with PBS solution twice. Cells were monitored and counted under confocal microscope (ZEISS, LSM710) after 1 mL Assay Buffer was added to the cells.

3.4 Histology and Immunohistochemistry

3.4.1 Formalin-fixed paraffin-embedded section mounting

Cat was sacrificed by lethal injection after all materials were implanted for 5/21/35 days. Tissues containing the material were incised into small blocks (about 1 cm ×1 cm ×0.5 cm). Tissue blocks were fixed with 4% (v/v) paraformaldehyde in 1 × PBS soltion at 4 □. Fixed tissues were processed for paraffin embedding which later were cut by a microtome (Leica RM 2135, Leica Microsystems Inc.) at a thickness of about 4 μm for the material.

3.4.2 Hematoxylin and Eosin (HE) staining, Masson's trichrome staining and immunohistochemical staining

Hematoxylin and Eosin Staining Kit (C0105, Beyotime Institute of Biology) was used for H&E staining, and Masson's Trichrome Staining Kit (G1006, Servicebio) was used for Masson's trichrome staining. For immunohistochemical staining, antigen retrieval was performed by heating in 0.01 M citrate buffer (pH 6.0). CD11b (1:300, ab133357, Abcam) was used as primary antibody and Cy3 conjugated goat anti-rabbit IgG (H+L) (1:300,

GB21303, Servicebio) was used as secondary antibody. H&E staining, Masson's trichrome staining and immunohistochemical staining were performed according to the manufacturer's instructions. H&E staining sections and Masson's trichrome staining sections were mounted with neutral resins and observed under microscope (Nikon Alphaphot-2®). Immunohistochemical sections were mounted with DAPI Fluoromount-G® (0100-20, Southern Biotech) and observed under confocal microscope.

4. Characterization

4.1 Structure characterization

The structures of SSFs were characterized by scanning electron microscope (Hitachi FE-SEM S-4800 operated at 1 kV). Gold nanoparticles were deposited at 110 mA for 30 s on the surface of the low-conductive materials.

The $SrPbBr_3$ nano dots (excitation: 488, emission: 525 nm) was synthesized *via* a sol-gel method[9]. And 1 mg/mL $SrPbBr_3$ toluene solution was incorporated into the PDMS precursor. Then the mixed solution was dip-coated onto the fibres to obtain a coating layer. Structures of the cross-section sample of single fibre and MSF sample was further verified by Scanning Laser Confocal Microscope (Nikon C2+).

4.2 Mechanical characterization

The mechanical properties of SSFs for long-term monitoring *in vivo* were test. The fibres were injected into the femoral vein of an adult cat (1.5–2.5 kg) and maintained in the blood vessel. After that, the SSFs were taken out by dissecting the blood vessel. Three SSFs were injected per day for five times and taken out on the last day. The mechanical properties of SSFs were measured using table-top universal testing instrument (10 N load cell; HY-0350). Each fibre with length of ~1.0 cm was fixed with tensile grip and stretched with a velocity of 20 mm/s.

The force of representative materials (including CNT fibre, silicon wire, gold wire, carbon fibre, tungsten wire, PET film, PI film and PDMS film) were tested by compressing at one end using table-top universal testing instrument (Zhongchen Inc, resolution ~ μN). Each material was placed with compression clamp and compressed with a velocity of 10 mm/s.

The nano indentation tests were performed using a Bruker Hysitron Ti-950 nanoindenter equipped with a standard Berkovich probe. In each test, 100 μN maximal normal force was

applied with 0.02 mN/s loading rate, followed by 2-second holding and 5-second unloading segment. The nano indentation hardness and reduced modulus were calculated from the unloading part in the load-displacement curve using Oliver-Pharr method.

The ultraviolet-visible spectrum was obtained *via* ultraviolet-visible spectrophotometer (Lambda 35, Perkin-Elmer). Poly(vinyl alcohol) (PVA)/PBS solution, residue PVA/PBS solution after flushing the fibre for over 30 days, random CNT dispersed in PVA/PBS solution were tested separately.

4.3 Photoacoustic test and 3D-reconstruction

All the photoacoustic tests and images were collected and analysed at the indicated time points with a Vevo LAZR Imaging System (Fuji Film VisualSonics Inc). Photoacoustic average signal of the CNT fibre was measured with a CNT fibre immersed in medical ultrasonic coupling agent with scanning wavelengths from 650 to 1000 nm.

4.3.1 The photoacoustic test of blood vessel injected with CNT fibre

The cat was anaesthetized by 3% isoflurane during the photoacoustic imaging and blood flow velocity test. The SSF was injected into the vein and the status of the fibre was continuously tested for 5 d. The coupling agent without air bubble was covered on the vein around the SSF for detection. To minimize the noise without affecting the intensity of signal, the photoacoustic gain was set at 27 dB and the B-Mode gain was set at 8 dB with a light wavelength of 726 nm in all tests. The 3D-mode test was done with a scanning velocity of 0.1 mm/s and a scanning length of 3.0 cm.

To obtain the coordinate information of the CNT fibre, the photoacoustic imaging video was transformed into a series of number matrix which indicated the strength of each pixel of the video ranging from 0 to 255. After removing all elements under 100, the region of interest was chosen to optimize the result. The broken line graph indicating five-day-change was plotted by linking their start, quarter, half, three quarters and end. All procedures were generated by MATLAB (**Figure 4c**).

The velocities of the blood flow with or without the SSF were measured. The SSF was injected into cat's femoral vein for five days. Similar to the photoacoustic test, the coupling agent without air bubble was covered on the vein around the SSF for detection and the velocity of the blood flow was tested by Acoustic Doppler Velocimeter. Another leg without

the fibre as the control group was measured with the same method.

4.3.2 The photoacoustic test of brain compression

To imitate pressure and force generated from the relatively movement from skull and brain, a compression force was applied on the cortex (**Figure 2e**). The medical ultrasonic coupling agent was carefully applied and photoacoustic test was then taken to obtain photoacoustic image of the brain under compression.

4.3.3 The photoacoustic test of cardiac muscle under twisting

The cardiac muscle with the fibre at a state of nature was used before twisting and then the muscle was rolled into an "S" shape after twisting (**Figure 2d □**). The medical ultrasonic coupling agent (being air-free) was carefully applied both on the surface and the gap in the twisting. And then photoacoustic test was conducted and recorded to acquire the photoacoustic image under twisting. The 3D-mode test was done with a scanning velocity of 0.1 mm/s and a scanning length of 3.0 cm.

The resulting data were treated as a three-dimensional structure by Vevo LAZR Imaging System. The signal was interrupted due to the penetration limit and extracted every 0.1 cm from the 3D image. Finally, all the signal images were re-built as **Figure 2d □**.

4.4 Electrochemical test

4.4.1 The performance of the SSFs

For the glucose, H_2O_2 and Ca^{2+} SSFs, the two-electrode system was studied. The SSF was used as the working electrode and the Ag/AgCl electrode served as both the reference electrode and counter electrode. The PSA SSF was measured by the three-electrode system with the sensing fibre as the working electrode, the Ag/AgCl as the reference electrode and the Pt as the counter electrode. The performances of glucose and H_2O_2 SSFs were tested with CHI600e (from Chenhua, Shanghai) in chronoamperometry at –0.42 V. The sensitivity was tested in the glucose/1×PBS solution with different concentrations, and the selectivity was tested by different solutions with similar molecular structure, such as D(+)-maltose, mannose, α-lactose, NAD+, hydrochloride, uric acid and ascorbic acid. The performance of Ca^{2+} SSF was tested in chronopotentiometry. The sensitivity of Ca^{2+} SSF was tested in the Ca^{2+} aqueous solution with different concentrations, and the selectivity was tested by different solutions with similar molecular structure, such as NH_4Cl, NaCl, $MgCl_2$ and KCl. The performance of Na^+ and K^+ SSFs was tested in the same method with Ca^{2+} SSF. The PSA SSF was

performed from –1.3 to 0 V with an increasing potential of 0.025 V in 1× PBS solution. The performance of pH SSF was tested in standard solutions with different pH. There were deviations in absolute potential and current values for sensors in the same solution. Thus calibration in standard solution to get a standard curve was necessary before testing. The reproducibility of SSF was measured with three samples under the same condition.

The definition of sensitivity was the current/voltage response caused by the certain concentration of the analyst. Therefore, the sensitivity was calculated by current/voltage change divided by concentration. For long-term test, normalized sensitivity was represented by the ratio of sensitivity at different days to the sensitivity of the first day.

4.4.2 The electrochemical performance of the H_2O_2 SSFs in agarose gel

Agarose (Sigma) was chosen as the diffusion model to form concentration gradient of H_2O_2. Agarose (3 wt%) was dissolved into water and heated at 150 □. After being dissolved completely, an MSF for spatial analysis was injected into the solution. The agarose solution with the sensing fibre was left at room temperature for 30 min to form MSF-embedded agarose gel. Then, 10 mL 10 wt% H_2O_2 (Sinopharm) aqueous solution was added on the top surface, and the diffusion process can be monitored by MSF. Before testing, conductive silver paint (SPI-PAINT) was coated on the outside end of each SSF for the connection to the electrochemical workstation (CHI660e). Each test contained 1-minute test on 5 SSFs of different depth and 5-minute break. After the tests in agarose gel were finished, agarose was melt and the device was taken out for further test in solution to obtain a standard curve for calibration.

4.4.3 The electrochemical stability in simulating body fluids under dynamic process

The electrochemical stability of the SSF was tested in simulating body fluids, and the test condition was decided based on the viscosity and velocity of the real body fluid. The two-electrode system was chosen with Ag/AgCl as both the counter and reference electrode and SSF as the working electrode. PVA/PBS solution was used to simulate the body fluids. Viscosity of the solution was tuned by the mass ration of PVA, ranging from 3 to 11 mPa·s. The test took place in the circulating pump and the velocity was regulated by the circulating pump from 40 to 100 mm/s.

PVA powder was dissolved in water at 80 °C overnight. Typically, a mixture with 11 mPa·s was made of 1.33 g PVA and 200 mL PBS. The mixture was poured into a silicon rubber tube

to cyclize under the circulating pump with a constant velocity of 80 mm/s. And the sensing fibre was injected like intravenous injection. Finally, conductive silver paint was coated on the outside end of SSF and reference electrode to test.

The electrochemical stability of the SSF was tested under dynamic process to simulate the body movement. The three-electrode system was chosen with Ag/AgCl, Pt and SSF as reference, counter and working electrodes, respectively. 1× PBS solution was chosen as the electrolyte. The electrochemical stability of the SSFs was test in A.C. impedance parameters with a frequency range of 1–100000 Hz. The stability of each SSF was tested after bending and twisting for total 100 cycles and each test was recorded every 10 cycles.

4.5 Electrochemical test *in vivo*

4.5.1 The fabrication of the integrated system

The conditioning path for each SSF was implemented in relation to the corresponding sensing mode. In the case of the amperometric-based glucose and H_2O_2 SSFs, the originally generated signal was collected in the form of electrical current. Therefore, a transimpedance amplifier was used to convert the signal current into voltage. In the case of the Ca^{2+} SSFs, the generated signals were essentially the voltage differences between the Ag/AgCl reference electrode and the working electrode of Ca^{2+} SSF. Therefore, we measured the difference in potential of the Ca^{2+} SSF and Ag/AgCl electrode directly. The details of conditioning path for each SSF are shown in **Figure S34.**

The whole circuit consists of conditioning path, amplifier, filter, Bluetooth module and user interface (**Figure S33**). A mobile application was designed to accompany the integrated system and to provide a user interface for data collection. After the MSF injection, conductive silver paint was coated between the device and the circuit.

4.5.2 Electrochemical measurement

4.5.2.1 The performance of MSF for spatial analysis *in vivo*

Seven-week female mice with different sizes of tumours from 80 to 1950 mm^3 were chosen as the experiment animals. To detect the distribution of H_2O_2 during tumour growth, the first day of test started with a tumour size of 80 mm^3, and we then tested the tumour size every 3 d. The distribution of H_2O_2 in mature tumours was tested every 4 h for over 20 h.

Key steps are described as follow. The mouse was anesthetized by isoflurane during each test

and was conscious between two adjacent tests. The MSF for spatial analysis was injected into the tumour tissue of a nude mouse as described in **Supplementary 2.4**. Each SSF was covered by conductive silver paint, connected to the circuit and tested in chronoamperometry at -0.42 V.

The simulation of the concentration was acquired by two dimensional Gaussian fitting based on five experimental data points we obtained. Centre of each tumour was defined from the optical photos. In the simulation, we assumed that dots with the same distances from their centres should have the same simulated concentration of H_2O_2, so the fitting function we used was listed as followed.

$$f(x,y) = \frac{1}{2\pi\sigma^2} exp[-\frac{1}{2\sigma^2}((x-\mu_1)^2 + (y-\mu_2)^2)]$$

Where σ was the standard deviation of the Gaussian fitting, x and y resembled the coordinate of the dot, and μ_1 and μ_2 resembled the coordinate of the centre.

4.5.2.2 The performance of MSF for multiplex monitoring *in vivo*

Five adult cats (1.5–2.5 kg) were chosen as the experiment animals. To detect the concentrations of Ca^{2+} and glucose in blood, the MSF was injected into the femoral vein for continuous monitoring at the same time.

The key experiment steps are described as follow. The cat was anesthetized by isoflurane during each test. The MSF for multiplex monitoring was injected into the femoral vein of a cat as described in **Supplementary 2.3**. Different doses of glucose and sodium chloride solution and calcium and sodium chloride solution (100 mM $CaCl_2$ and 154 mM NaCl solution) were injected into another femoral vein of the animal to raise the blood glucose and calcium level, respectively. Each test had been taken for more than 2 h. The Ca^{2+} SSFs and ZnO-based glucose SSFs were test *in vivo* for 28 days.

4.5.2.3 Verification of the fidelity of sensor

To prove the accuracy of the test, the blood glucose of the cat was measured by a commercial glucose meter (On Call EZ2, ACON Biotech (Hangzhou)) and the blood calcium was measured by the commercial calcium assay kit (K380-250, Biovision). Both blood samples were collected from the auricular veins of the cats by a blood lancet. The blood glucose was measured during the test by dipping blood sample into the reaction groove and data were exported immediately. Blood samples for blood calcium test were collected during the test by dipping the blood (10 μL) into a heparin-treated eppendorf tube. After the test was finished,

the commercial calcium assay kit was used to measure the calcium in the blood sample by spectrophotometry. The blood samples (10 μL) were diluted with 40 μL distilled water and then mixed with 90 μL Chromogenic Reagent and 60 μL Calcium Assay Buffer, and then the mixture stood still for 10 min. OD575 was measured by NanoDrop 8000. The calibration curve was acquired by the standard sample in the kit. The blood samples were stored at 4 °C between the test and measurement.

5. Calculation and simulation

5.1 Bending stiffness

To calculate the bending stiffness (*D*), a fixed boundary was set as one of the ends parallel with the bending direction, and a small vertical displacement, *d*, is added on the end. The bending stiffness can be defined as

$$D = EI$$

where *E* and *I* represent elastic modulus and moment of inertia, respectively.

For a beam of rectangular cross section with width *b* and height *h*, the moment of inertia is

$$I = \frac{bh^3}{12}$$

For a circular cross section of diameter *d*,

$$I = \frac{\pi d^4}{64}$$

5.2. Mises stress of assembled fibre upon bending

Though the CNTs were based on nano-scale, the laws of continuum mechanics were still robust and applicable[10,11]. Moreover, when the aspect ratio of fibres was relatively large, the CNTs can be treated as simple continuum beam models [12-14], which significantly reduces the computation cost compared with atomistic models.

Parallel-arranged, no sliding fibres were considered to simplify the hierarchical model[Error! Reference source not found.] **(Figure S8)**. To explain how the structure of the CNT fibres affects their macroscopic properties, we applied finite element method using software ABAQUS [16] to simulate the deformation of CNT fibres with the length *L=25* μm and the diameter of cross section d=*50* nm. The elastic modulus and Poisson's ratio of CNT were 1 TPa and 0.3, respectively. Besides, van der Waals interaction played a key role between two CNTs [10-13], and Tang et al.[Error! Reference source not found.] predicted the equilibrium separation between two parallel

CNTs is 3.5 Å. For different hierarchical CNT bundles, we defined the void ratio of cross section as the void area over the entire cross section area:

$$\phi = \frac{S_{\mathrm{V}}}{S} = \frac{\pi d^2 - n\pi d_b^2}{\pi d^2} = 1 - n(d_b/d)^2$$

where d_b is the diameter of CNT bundle, and n is the number of CNT bundles in the cross section. Here, we considered the calculated void ratios listed in the table below.

d_b (nm)	50	17	10	7.06	5.5	4.46	3.5
n	1	7	19	37	61	91	127
ϕ	0	0.1908	0.24	0.2619	0.2629	0.2748	0.3777

In the simulation, beam elements (B31) were applied to discretize the CNT bundles. Inspired by Huang et al.[Error! Reference source not found.], we used spring elements to represent the van der Waals interaction. Considering both axial and radial van der Waals interplay, oblique distributed linear springs were employed in the interaction between adjacent CNTs. Taking Hamaker constant $A=10^{-19}$ *J* as a typical value, the van der Waals energy of parallel cylinders or rods of radii R_1 and R_2 (per unit length) can be expressed as[19]

$$W = \frac{-A}{12\sqrt{2}\,X^{3/2}}\left(\frac{R_1 R_2}{R_1 + R_2}\right)^{1/2}$$

which leads to the van der Waals Force

$$F = -\frac{dW}{dX} = \frac{-A}{8\sqrt{2}\,X^{5/2}}\left(\frac{R_1 R_2}{R_1 + R_2}\right)^{1/2}$$

where X denotes a distance between separated surfaces. Considering the first two terms of its Taylor series expanded at the initial distance X_0, one obtains

$$\begin{aligned} F(X) &\approx F(X_0) + F'(X_0)\cdot(X - X_0) \\ &\approx F(X_0) + \left(\frac{5A}{16\sqrt{2}}\left(\frac{R_1 R_2}{R_1 + R_2}\right)^{1/2} X_0^{-\frac{7}{2}}\right)\cdot(X - X_0) \end{aligned}$$

By analogy with classical spring model:

$$F_2 - F_1 = k\cdot(x_2 - x_1)$$

we have

$$k \approx \left(\frac{5A}{16\sqrt{2}} \left(\frac{R_1 R_2}{R_1 + R_2} \right)^{1/2} {X_0}^{-\frac{7}{2}} \right)$$

where *k* denotes the spring stiffness.

When subjected to axial compression, the CNT fibre may undergo nonlinear buckling response. To predict buckling behaviour of CNT fibres, Riks algorithm is adopted to obtain nonlinear equilibrium solutions for the overall buckling process of CNT fibres.

5.3. Mises stress of the fibre embedded in tissue

The fibres implanted in the tissue deform with the vicinity under different loads. Considering the practical application, excessive stress on the interface between two materials may cause damage even tearing of tissue. To look into the deformation at interface and to predict the stress distribution, we established finite element models with various geometries and loads.

To solve large deformations of fibre-embedded tissues, a pseudo-dynamic algorithm (a stabilized nonlinear resolution method in finite element software ABAQUS) was used for two types of loading, i.e. twisting (**Figure S11**) and bending (**Figure S12**). In the simulation, the elastic modulus and Poisson's ratio of medium are 480 MPa and 0.3, respectively, which is equivalent to the muscle [20]. For comprehensive analysis, we choose different types of fibres to implant in the medium, including CNT fibre (2.0 GPa, 0.3), carbon fibre (290 GPa, 0.3), tungsten wire (400 GPa, 0.28), and gold wire (77 GPa, 0.42). The diameter of fibres is 50 μm, and the length is 10 mm. Besides, widely used polymer films were taken into account, including PET (2.6 GPa, 0.4) and PI (23 GPa, 0.33) with thickness of 50 μm, width of 5 mm, and length of 10 mm. In addition, the maximum Mises stress on the interface is plotted in **Figure S11 (c)** (twisting) and **Figure S12 (c)** (bending).

Supplementary References

1. Liu, P. et al. Stretchable and energy□efficient heating carbon nanotube fibre by designing a hierarchically helical structure. *Small* **14**, 1702926 (2018).
2. Lee, H. et al. Wearable/disposable sweat-based glucose monitoring device with multistage transdermal drug delivery module. *Sci. Adv.* **3**, e1601314 (2017).
3. Tarlani, Aliakbar, *et al*. New ZnO nanostructures as non-enzymatic glucose biosensors. *Biosens Bioelectron.* **67**, 601-607 (2015).
4. Gao, W. *et al.* Fully integrated wearable sensor arrays for multiplexed in situ perspiration analysis. *Nature.* **529**, 509–514 (2016).
5. Tang, Z., Fu, Y. & Ma, Z. Bovine serum albumin as an effective sensitivity enhancer for peptide-based amperometric biosensor for ultrasensitive detection of prostate specific antigen. *Biosens. Bioelectron.* **94**, 394-399 (2017).
6. Lee, Hyuk Jin, et al. Solvent-processible polymer membrane-based liquid junction-free reference electrode. *Anal Chem*. **70**,16 (1998).
7. Chen, P. et al. Hierarchically arranged helical fibre actuators driven by solvents and vapours. *Nat. Nanotechnol.* **10**, 1077 (2015).
8. Liu, J. et al. Syringe-injectable electronics. *Nat. Nanotechnol.* **10**, 629 (2015).
9. Song, J. et al. Room□Temperature Triple□Ligand Surface Engineering Synergistically Boosts Ink Stability, Recombination Dynamics, and Charge Injection toward EQE□11.6% Perovskite QLEDs. *Adv. Mater*. **30**, 30 (2018).
10. He, X. Q., et al. Buckling analysis of multi-walled carbon nanotubes: a continuum model accounting for van der Waals interaction. *J. Mech. Phys. Solids* **53**, 303-326 (2005).
11. Ru, C. Q. Effect of van der Waals forces on axial buckling of a double-walled carbon nanotube. *J. Appl. Phys.* **87**, 7227-7231 (2000).
12. Natsuki, T., et al. Stability analysis of double-walled carbon nanotubes as AFM probes based on a continuum model. *Carbon* **49**, 2532-2537 (2011).
13. Timesli, A., et al. Prediction of the critical buckling load of multi-walled carbon nanotubes under axial compression. *C. R. Mec.* **345**, 158-168 (2017).
14. Khosravian, N, and H. Rafii-Tabar. Computational modelling of a non-viscous fluid flow in a multi-walled carbon nanotube modelled as a Timoshenko beam. *Nanotechnology* **19**, 275703 (2008).
15. Sun, H., et al. Energy harvesting and storage in 1D devices. *Nat. Rev. Mater*. **2**, 17023 (2017).
16. ABAQUS, *ABAQUS Analysis Users Manual*, version 6.13, 2013.

17. Tang, T., et al. Adhesion between single-walled carbon nanotubes. *J. Appl. Phys.* **97**, 787 (2005).
18. Huang, S. Q., et al. Pattern instability of a soft elastic thin film under van der Waals forces. *Mech. Mater.* **38**, 88-99 (2006).
19. Israelachvili, J. N., Intermolecular and surface forces. Academic Press. (2011).
20. R. Feiner, and T. Dvir. Tissue–electronics interfaces: from implantable devices to engineered tissues. *Nat. Rev. Mater.* **3**, 17076 (2017).

Table S1. Calculated bending stiffness of implantable devices and tissues with the moduli measured by indentation method.

	Material	**Geometry and size**	**Modulus (Indentation)***	**Bending stiffness (nN m^2)**	**Reference**
Devices	gold	Wire Diameter: 10–1000 μm	74.08±1.44 GPa	3.63×10^{-2}–3.63×10^{6}	Measured
	Carbon fibre	Fibre Diameter: 5–10 μm	17.5±1.06 GPa	5.37×10^{-4}–8.59×10^{-3}	Measured
	Silicon	Shank# Width: 20–144 μm Thickness:14.75–100 μm	134±1.31 GPa	7.17×10^{-1} –1.61×10^{3}	Measured
Tissues	Nervous system	5–20 μm	0.2–7 kPa	6.13×10^{-12}–5.40×10^{-8}	[1], [2]
	Skin		~85 kPa	2.60×10^{-9}–6.67×10^{-7}	[3], [4], [5]
	Muscle		~7 kPa	2.15×10^{-10}–5.50×10^{-8}	[6], [7]
	Blood vessel		~125 kPa	3.83×10^{-9}–9.81×10^{-7}	[7], [8], [9], [10]
Sensing fibre	CNT fibre	Fibre Diameter: 1–50 μm	118.9±3.5 MPa	5.66×10^{-9}–3.75×10^{-2}	Measured

* The moduli measured by indentation method were produced usually by atomic force microscopy or nanoindentation facilities to reveal the properties at cellular scale[11].

The dimensions of silicon-based electronic devices range from 14.75 to 144 μm. The bending stiffness of silicon was calculated by the pillar model with a section dimension from 20 μm×14.75 μm to 144 μm×100 μm.

Reference at Table S2

1. MacManus, D. B., Murphy, J. G. & Gilchrist, M. D. Mechanical characterisation of brain tissue up to 35% strain at 1, 10, and 100/s using a custom-built micro-indentation apparatus. *J. Mech. Behav. Biomed. Mater.* **87,** 256–266 (2018).
2. Chen, R., Canales, A. & Anikeeva, P. Neural recording and modulation technologies. *Nat. Rev. Mater.* **2,** 16093 (2017).

3. McFarland, M., Smith, J. F., Constantinides, G., Van Vliet, K. J. & Kalcioglu, Z. I. Probing mechanical properties of fully hydrated gels and biological tissues. *J. Biomech.* **41,** 3285–3289 (2008).
4. Zheng, Y. P., Choi, Y. K. C., Wong, K., Chan, S. & Mak, A. F. T. Biomechanical assessment of plantar foot tissue in diabetic patients using an ultrasound indentation system. *Ultrasound Med. Biol.* **26,** 451–456 (2000).
5. Chiu, S. K. W. *et al.* Quantitative measurement of post-irradiation neck fibrosis based on the young modulus. *Cancer* **95,** 656–662 (2002).
6. Chen, E. J., Novakofski, J., Jenkins, W. K. & O'Brien, W. D. Young's modulus measurements of soft tissues with application to elasticity imaging. *IEEE Trans. Ultrason. Ferroelectr. Freq. Control* **43,** 191–194 (1996).
7. Engler, A. J., Richert, L., Wong, J. Y., Picart, C. & Discher, D. E. Surface probe measurements of the elasticity of sectioned tissue, thin gels and polyelectrolyte multilayer films: Correlations between substrate stiffness and cell adhesion. *Surf. Sci.* **570,** 142–154 (2004).
8. Ebenstein, D. M. & Pruitt, L. A. Nanoindentation of soft hydrated materials for application to vascular tissues. *J. Biomed. Mater. Res. Part A* **69,** 222–232 (2004).
9. Jacot, J. G., Dianis, S., Schnall, J. & Wong, J. Y. A simple microindentation technique for mapping the microscale compliance of soft hydrated materials and tissues. *J. Biomed. Mater. Res. Part A* **79A,** 485–494 (2006).
10. Oie, T. *et al.* Local elasticity imaging of vascular tissues using a tactile mapping system. *J. Artif. Organs* **12,** 40–46 (2009).
11. McKee, C. T., Last, J. A., Russell, P. & Murphy, C. J. Indentation Versus Tensile Measurements of Young's Modulus for Soft Biological Tissues. *Tissue Eng. Part B Rev.* **17,** 155–164 (2011).

Table S2. Calculated bending stiffness of state-of-art implantable devices and tissues with tensile moduli.

Device	Material	Geometry and size	Modulus (Tensile) *	Bending stiffness ($nN\ m^2$)	Reference
Ultra small electrode for neural interface	Carbon fibre	Fibre diameter: 7 μm	234 GPa	0.028	[1]
E-dura for neural interface	PDMS	Film Width: 3 mm Thickness:120 μm	100 kPa	0.43	[2]
Syringe-injectable electronics	SU-8/Gold	Mesh Width: 20 μm Thickness: 1 μm	/	2.8×10^{-6}	[3]
Neuron-like electronics	SU-8/Gold	Mesh Width: 1-4 μm Thickness: 1 μm	/	1.4×10^{-7}–5.7×10^{-7}	[4]
Multifunctional fibre for neural interface	PC	Fibre Diameter: 70 μm	1.7 GPa	2.0	[5]
Neuropixels	Silicon	Wire Width: 70 μm Thickness: 20 μm	165 GPa	7.7	[6]
Implantable optoelectronics	PDMS embedded with LED	Film Width: 3.8 mm Thickness: 0.7 mm	1.7 GPa	1.85×10^{5}	[7]
Implantable optoelectronics	PDMS	Film Width: 3.8 mm Thickness: 0.7 mm	0.5 MPa	54.3	[7]
Needle shaped piezoelectric microsystem for diagnosis	Polyimide	Needle Width: 0.5 mm Thickness: 75 μm	2 GPa	35.2	[8]
Tissues	Nervous	5-20 μm	2 MPa	6.13×10^{-8}–1.57×10^{-5}	[9]

	system				
	Skin		60 MPa	1.84×10^{-6}–4.71×10^{-4}	[10]
	Muscle		480 MPa	1.47×10^{-5}– 3.77×10^{-3}	[11]
	Blood vessel		6.85-15.69 MPa	2.1×10^{-7} –1.23×10^{-5}	[12]
Sensing fibre	CNT fibre	Fibre Diameter: 1-50 μm	Average of ~4 GPa	1.96×10^{-7} –1.23	This work

* The moduli under tensile were tested usually by tensile method to reveal the macroscopic mechanical properties of materials and tissues.

Reference in Table S3:

1. Yoshida Kozai, T. D. *et al.* Ultrasmall implantable composite microelectrodes with bioactive surfaces for chronic neural interfaces. *Nat. Mater.* **11,** 1065–1073 (2012).
2. Minev, I. R. *et al.* Electronic dura mater for long-term multimodal neural interfaces. *Science.* **347,** 159–163 (2015).
3. Liu, J. *et al.* Syringe-injectable electronics. *Nat. Nanotechnol.* **10,** 629–636 (2015).
4. Yang, X. *et al.* Bioinspired neuron-like electronics. *Nat. Mater.* **18,** 510–517 (2019).
5. Canales, A. *et al.* Multifunctional fibers for simultaneous optical, electrical and chemical interrogation of neural circuits in vivo. *Nat. Biotechnol.* **33,** 277–284 (2015).
6. Jun, J. J. *et al.* Fully integrated silicon probes for high-density recording of neural activity. *Nature* **551,** 232–236 (2017).
7. Park, S. Il *et al.* Soft, stretchable, fully implantable miniaturized optoelectronic systems for wireless optogenetics. *Nat. Biotechnol.* **33,** 1280–1286 (2015).
8. Yu, X. *et al.* Needle-shaped ultrathin piezoelectric microsystem for guided tissue targeting via mechanical sensing. *Nat. Biomed. Eng.* **2,** 165–172 (2018).
9. Prange, M. T. & Margulies, S. S. Regional, Directional, and Age-Dependent Properties of the Brain Undergoing Large Deformation. *J. Biomech. Eng.* **124,** 244 (2002).
10. Edwards, C. & Marks, R. Evaluation of biomechanical properties of human skin. *Clin. Dermatol.* **13,** 375–380 (1995).
11. McKee, C. T., Last, J. A., Russell, P. & Murphy, C. J. Indentation Versus Tensile Measurements of Young's Modulus for Soft Biological Tissues. *Tissue Eng. Part B Rev.* **17,** 155–164 (2011).
12. Fung, Y.-C. Mechanical Properties and Active Remodeling of Blood Vessels.

Biomechanics 321–391 (Springer New York, 1993).

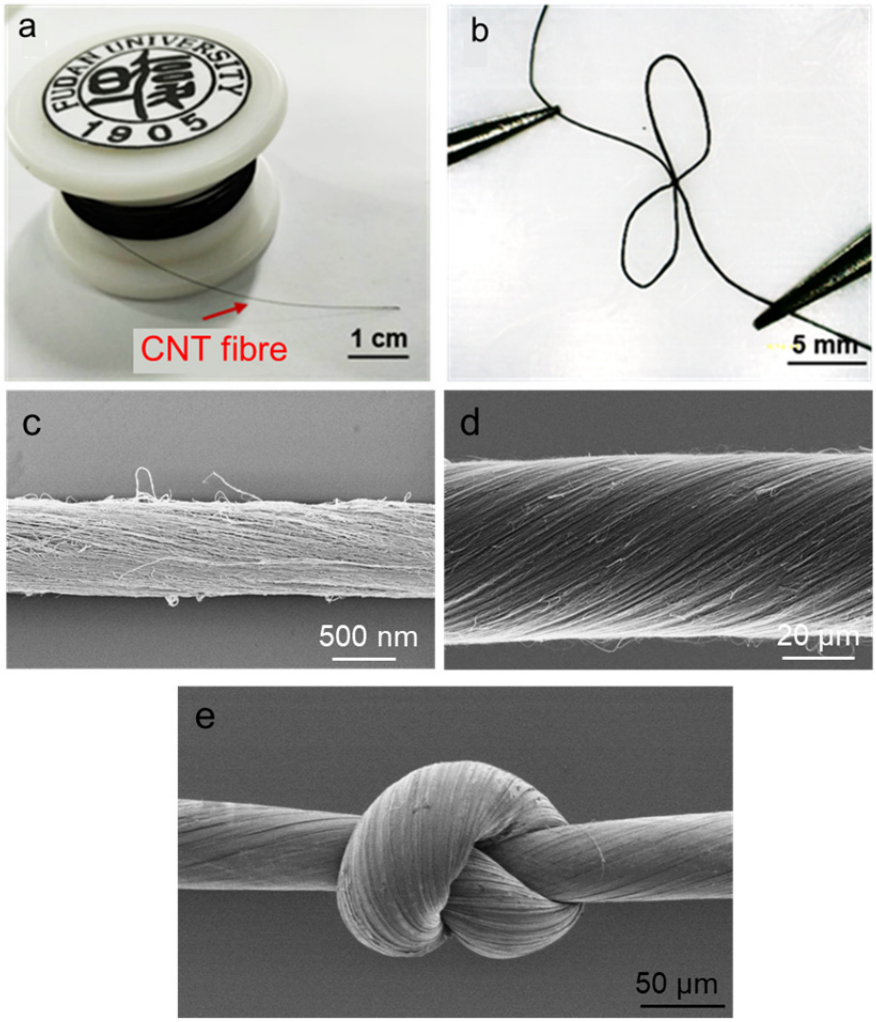

Figure S1. a, Photograph of a roll of CNT fibre (technical repeats>100). **b**, Photograph of a knotted CNT fibre (technical repeats=5). **c** and **d**, SEM images of aligned CNT fibres with different diameters (technical repeats=5). **e**, SEM image of a knotted CNT fibre showing the stability under the external force (technical repeats=5).

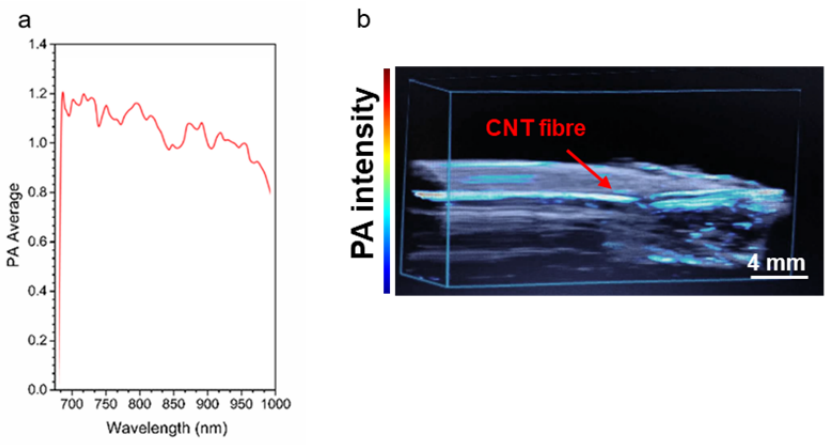

Figure S2. a, Photoacoustic average signal of the CNT fibre at the wavelength range of 700–1000 nm. **b**, Photoacoustic 3D-reconstruction image of the tissue after the CNT fibre injected into a femoral vein of a cat for 5 days. The colour line is the photoacoustic signal of the CNT fibre.

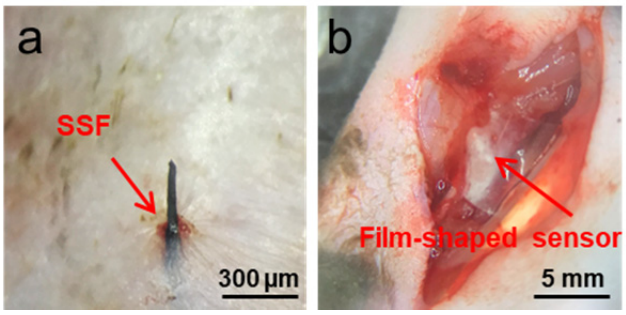

Figure S3. Representative optical images of the wounds with different implant methods. **a**, Syringe-assisted injection of SSF into a femoral vein of a cat (technical repeats=5). **b**, Surgical insertion of film-shaped sensor into a hind leg of a cat (technical repeats=3).

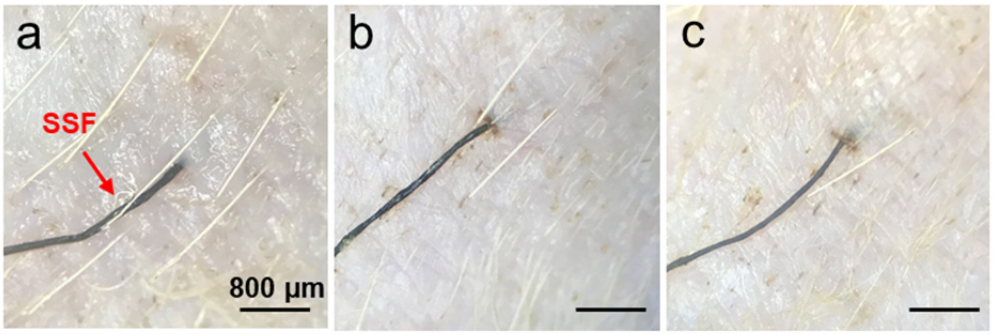

Figure S4. Representative optical images of the injected SSF on the skin of a cat for (**a**) 1 day, (**b**) 2 days and (**c**) 4 days, showing no inflammation in all cases (technical repeats=4).

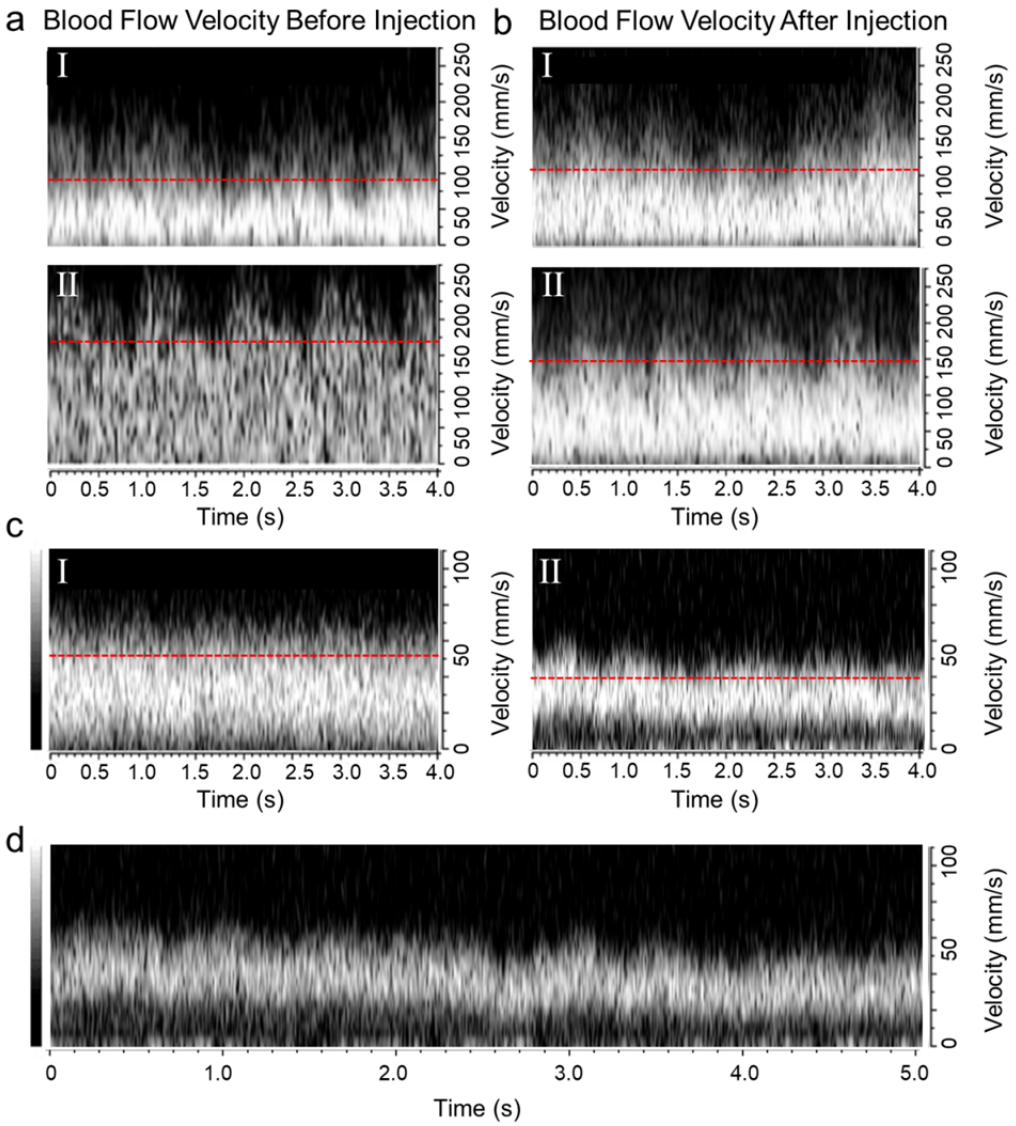

Figure S5. a and **b,** Comparison of blood flow velocities before and after the CNT fibre injection into blood vessel of 2 cats for 5 days, respectively. **c,** The blood flow velocities of a typical blood vessel at different time points of 0 and 6 hours in a normal cat without CNT fibre, showing a physiological fluctuation across long term. **d**, The blood flow velocity of a typical blood vessel of a normal cat at the initial 5 seconds, showing a physiological fluctuation across short term. All data were collected from 3 cats and the red lines represented the mean blood flow velocity during test. The blood flow velocity normally fluctuates, and the visible increase (a) or decrease (b) after implantation was not necessarily related to CNT fibre injection.

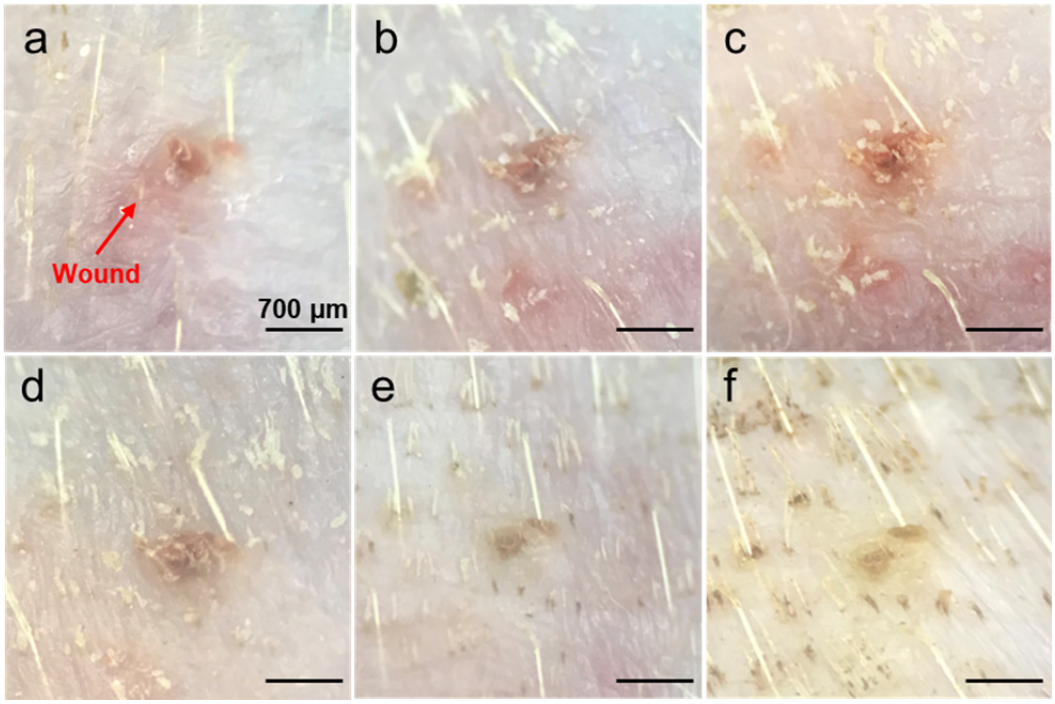

Figure S6. Representative optical images of the wound on skin surface of a cat after removal of the SSF healing for (**a**) 0 hour, (**b**) 2 hours, (**c**) 4 hours, (**d**) 6 hours, (**e**) 24 hours and (**f**) 48 hours (technical repeats=5).

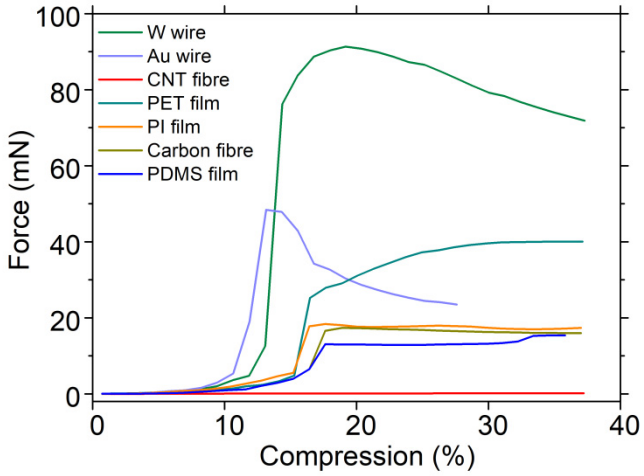

Figure S7. Representative internal force generation curves under compression for different materials (technical repeats=3). The diameters of the tungsten (W) wire, gold (Au) wire, carbon fibre (CF) and CNT fibre is ~50 μm. The section sizes of the polyethylene terephthalate (PET) film, polyimide (PI) film and PDMS film are 50 μm × 5 mm. The lengths of all the materials are 4 mm.

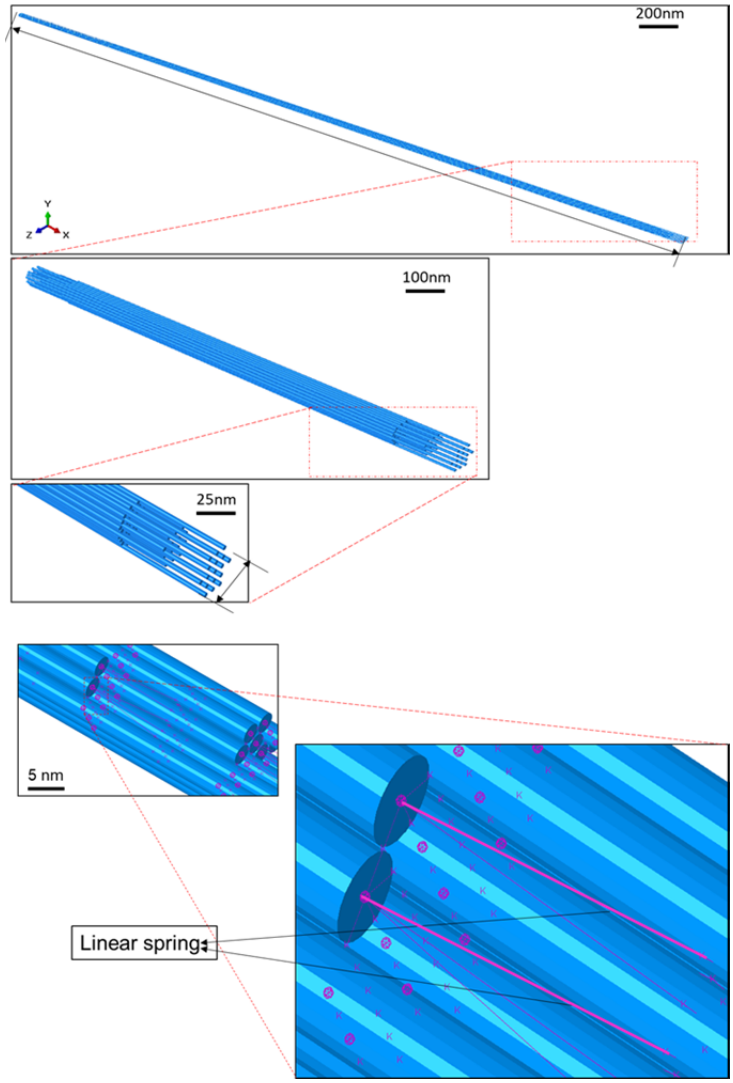

Figure S8. The model of the CNT fibre being hierarchically assembled.

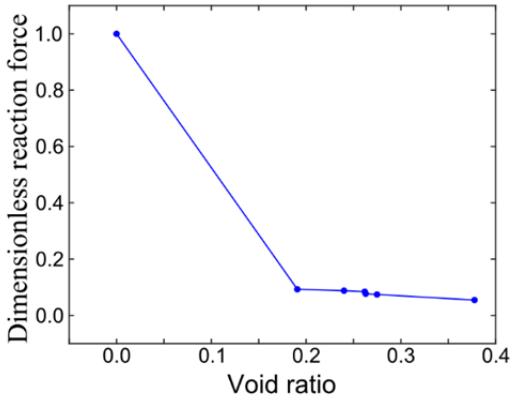

Figure S9. The computed force for CNT fibres with different void ratios under compression. The dimensionless reaction force varied at different void ratios.

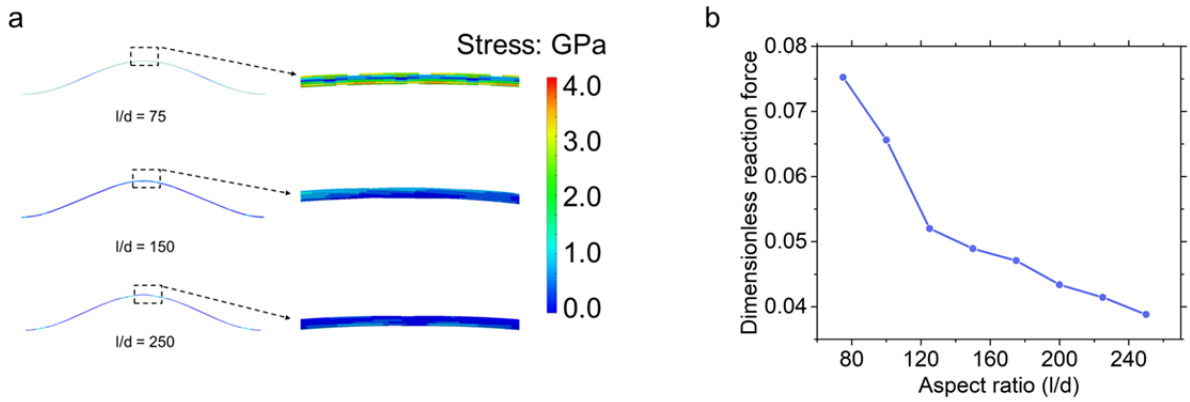

Figure S10. The simulation of CNT fibres with different aspect ratios of nanotubes. **a,** The distribution of stresses under different aspect ratios. **b,** The dimensionless reaction forces varied at different aspect ratios.

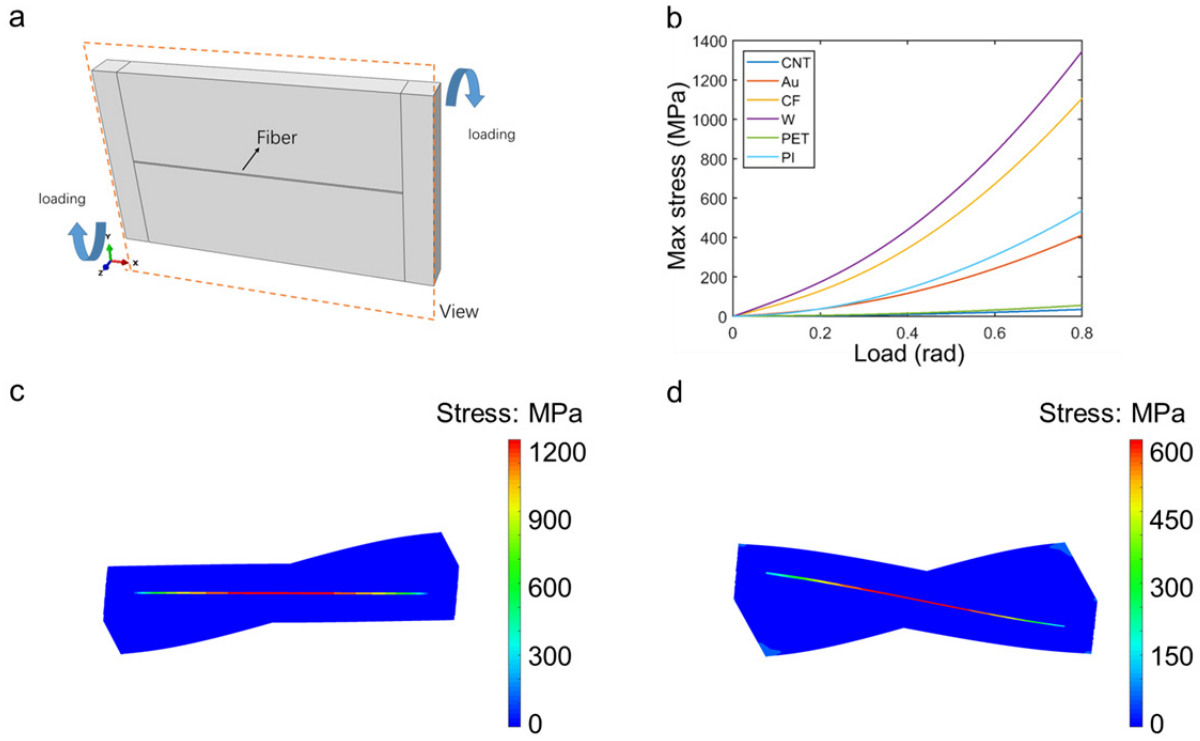

Figure S11. The calculated stress of the CNT fibre and the other implantable materials in a medium similar to tissue under twisting. **a**, Schematic of twist at the ends. **b**, The maximum Mises stress under different twisting angles varied for different implantable materials. **c,** The stress distribution of carbon fibre in medium. **d,** The stress distribution of PI film in medium.

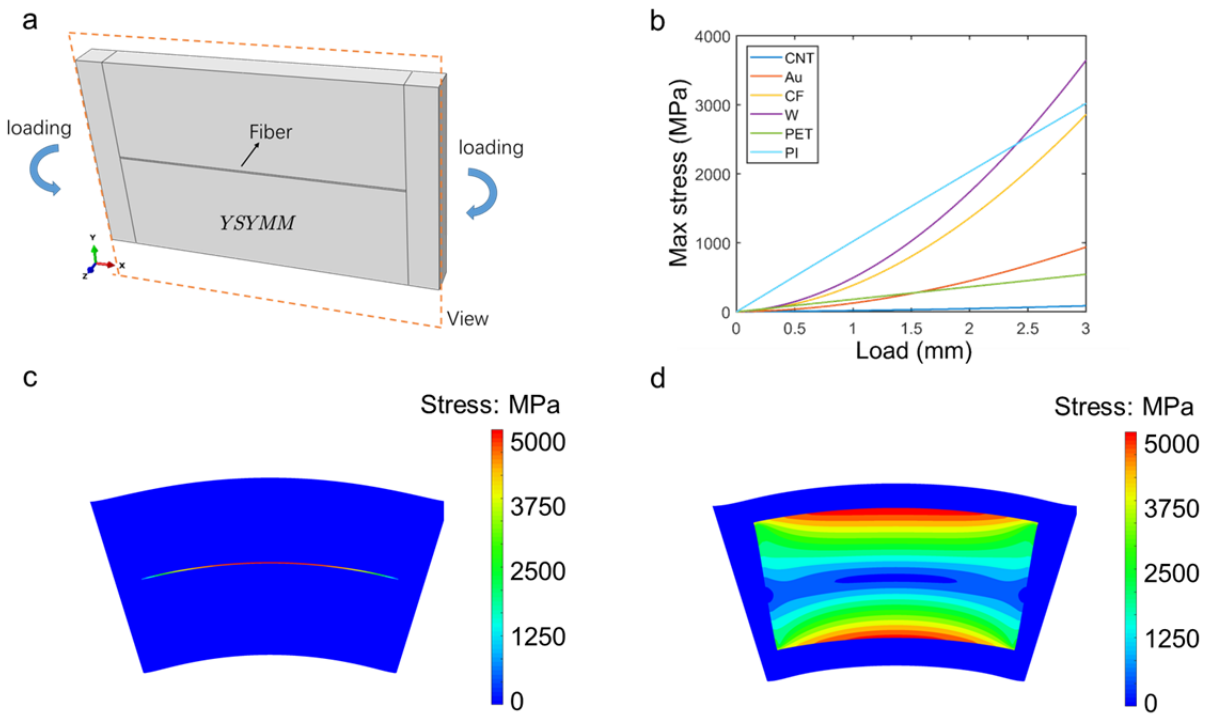

Figure S12. The simulated stress of the CNT fibre and the other implantable materials in a medium similar to tissue under bending. **a**, Schematic of the bending at the ends. **b**, The stress under different bending angles varied for different implantable materials. **c,** The stress distribution of carbon fibre in medium. **d,** The stress distribution of PI film in medium.

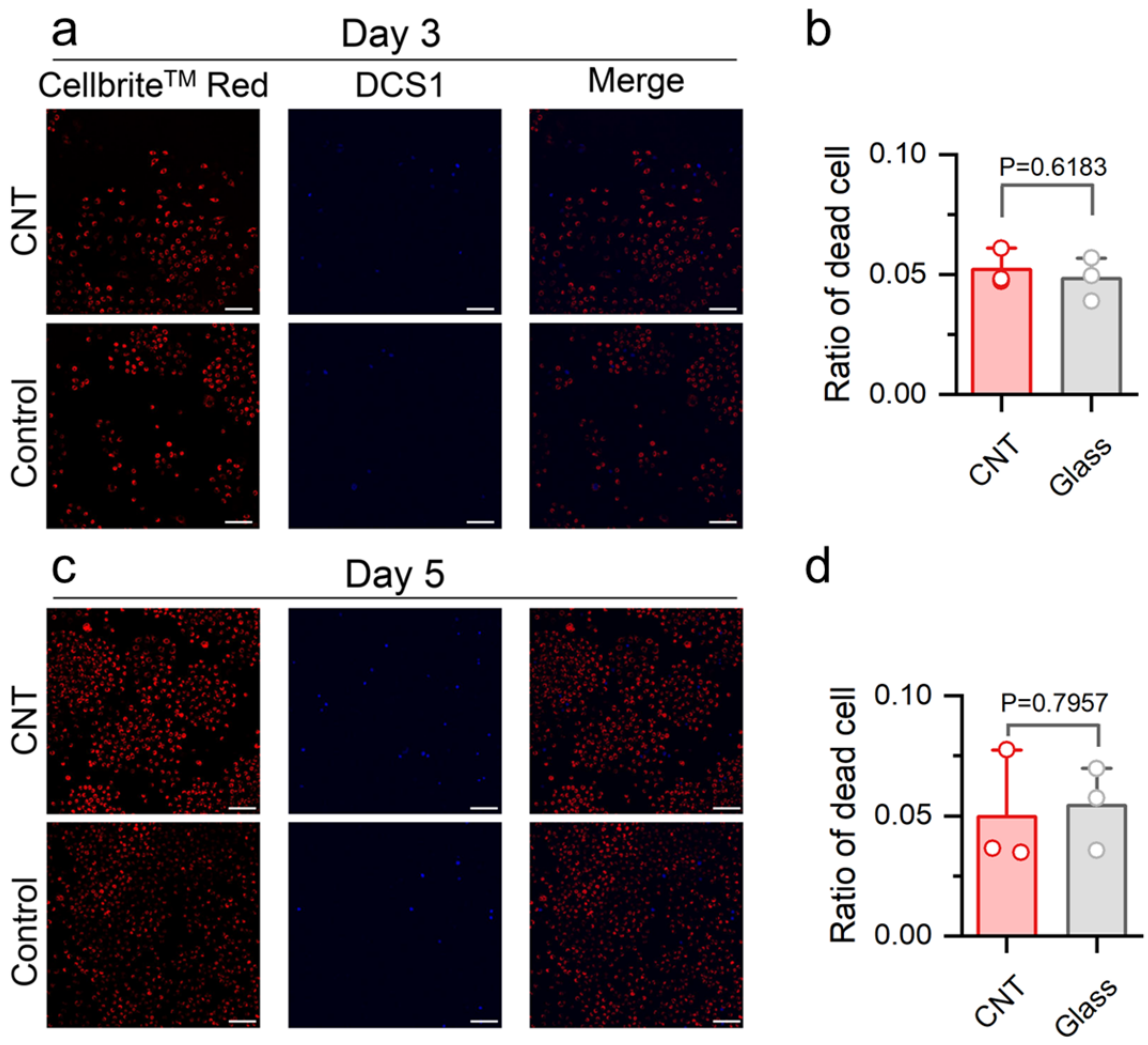

Figure S13. The effect of CNTs on the proliferation of fibroblast L929 cells. Representative confocal images of Cellbrite™ Red and Nuclear Blue™ DCS1 stained proliferating L929 cells cultured 3 days (**a**) and 5 days (**b**) on CNTs and glasses as control (technical repeats=3). Red: living cells, Cellbrite™ Red, blue: dead cells, Nuclear Blue™ DCS1. Quantitative measurement of Cellbrite™ Red stained cell number of CNTs and control group for 3 days (**c**) and 5 days (**d**). P value was calculated using One-way ANOVA.

Raw data for Figure S13b:

Raw data	Day 3					
	CNT			Control		
Experiment	1	2	3	1	2	3
Dead cell number	5	4	4	3	5	4
Live cell number	82	85	83	77	88	81
Total cell number	87	89	87	80	93	85
Dead cell ratio	0.06098	0.04706	0.04819	0.03896	0.05682	0.04938

Raw data for Figure S13d:

Raw data	Day 5					
	CNT			Control		
Experiment	1	2	3	1	2	3
Dead cell number	4	11	5	5	4	9
Live cell number	115	142	137	87	112	129
Total cell number	119	153	142	92	116	138
Dead cell ratio	0.03478	0.07746	0.0365	0.05747	0.03571	0.06977

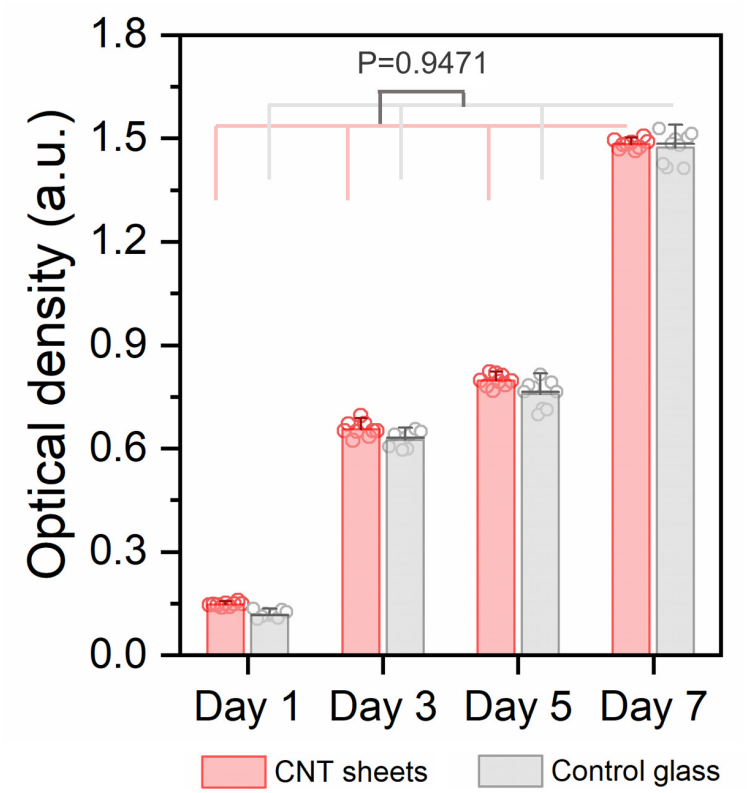

Figure S14. Cell proliferation of fibroblast cell L929 on CNT and glass (control) substrates over 7 days (n=9, technical repeats=3); P values was calculated using paired t test. P=0.9471 indicates no significant difference statistically.

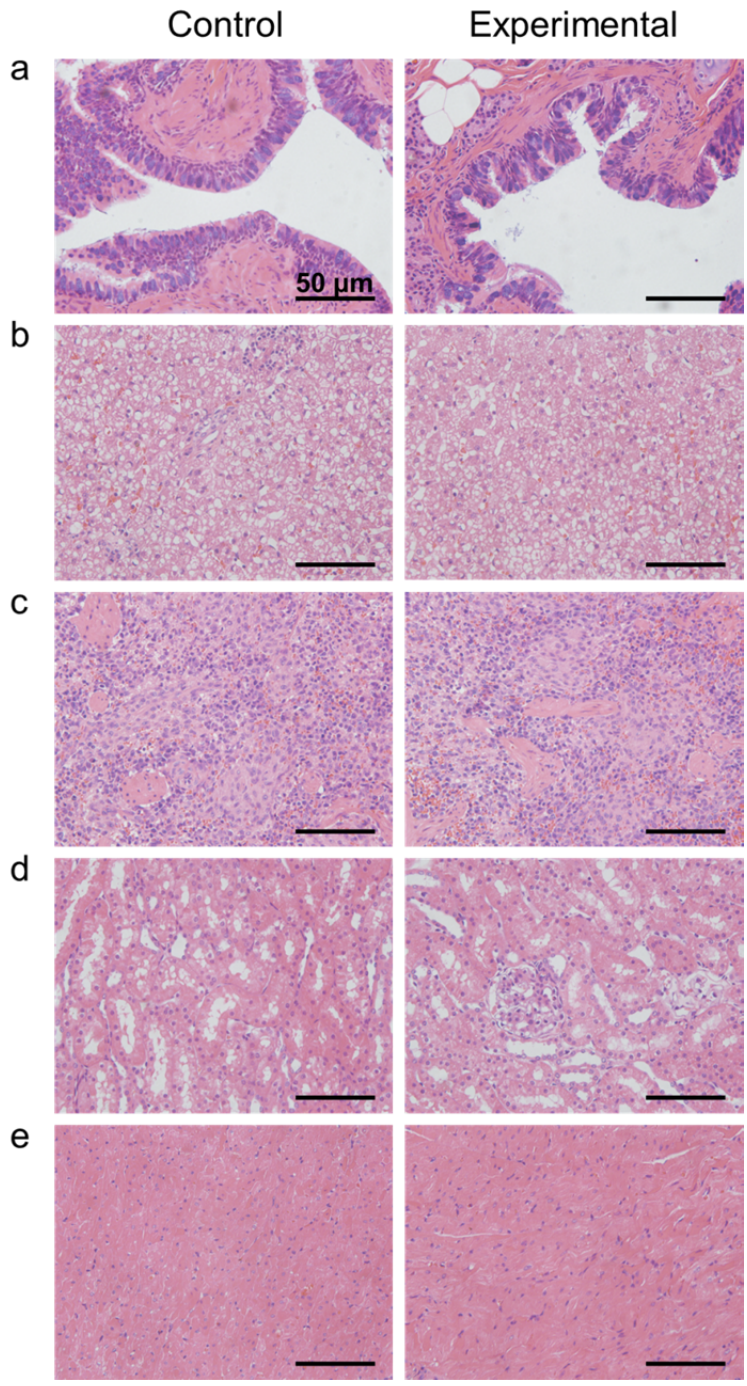

Figure S15. Optical images of HE staining of one typical slice from (**a**) lung, (**b**) liver, (**c**) spleen, (**d**) kidney and (**e**) cardiac muscle in control (left) and CNT fibre implanted group (right). It is notable that no CNT residues could be found in both groups, indicating that the CNT did not show tissue toxicity after 21 days' implantation. For each organ of cat, 9 sites were randomly selected and checked separately and the results were similar.

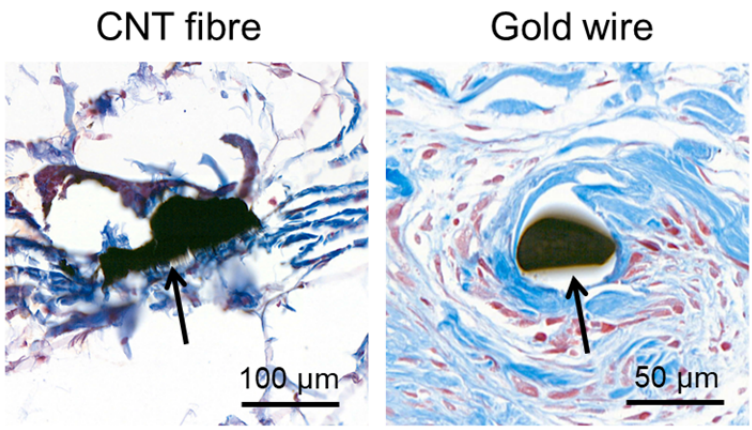

Figure S16. Representative Masson's trichrome staining sections with CNT fibre and gold wire after 21 days' implantation (technical repeats=3). The black arrows indicate the position of CNT fibre and gold wire. Red: cytoplasm, muscle and erythrocytes; blue: collagen; dark blue: nucleus.

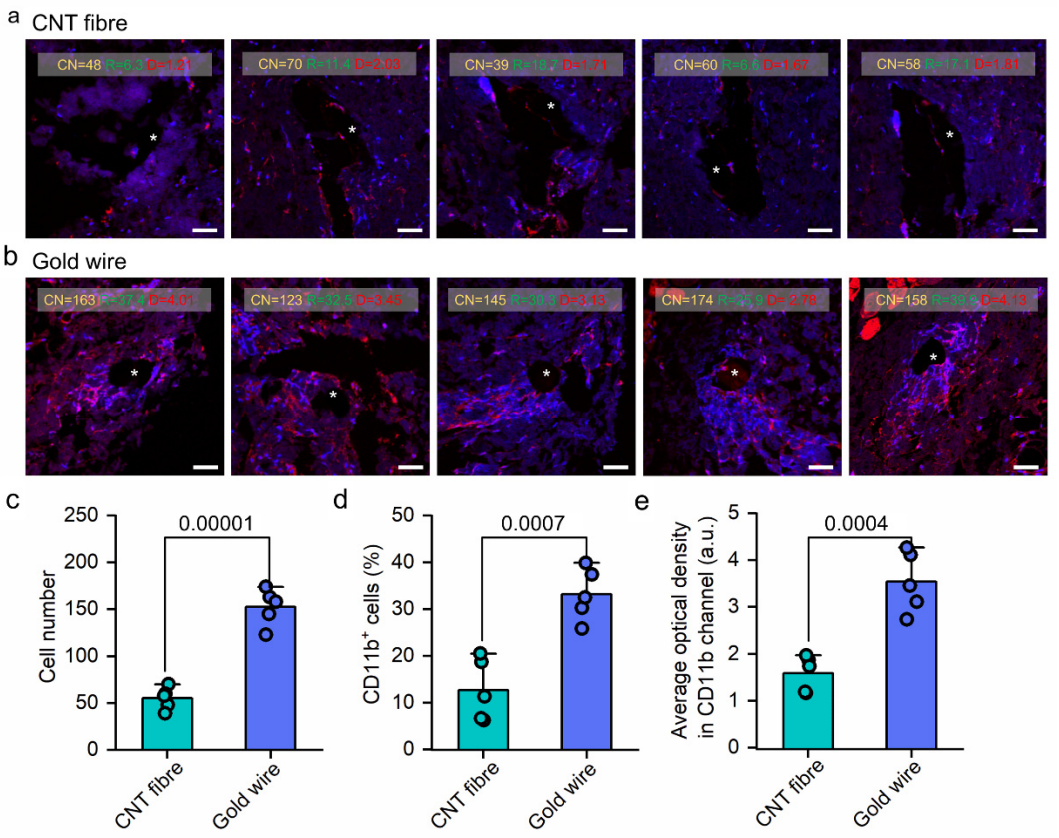

Figure S17. **a** and **b**, Confocal images of immunochemical labelled sections with CNT fibre and gold wire after implantation for 5 days (5 sites for each). Scale bars, 20 μm. CN represents the cell number, R represents the percentage of CD11b labelled ($CD11b^+$) cells over all cells and D represents the average optical density in red channel. The white asterisk indicates the implanted site. Blue: nucleus, DAPI; red: CD11b. **c**–**e**, Quantitative analysis of cell number, percentage of $CD11b^+$ cells and average optical density of CD11b based on raw data listed above the images in **a** and **b** (n=5 biologically independent experiments). All data were expressed as the mean ± s.d. Statistical differences among the groups were determined by two-sided *t*-test, with *P* values indicated on the charts.

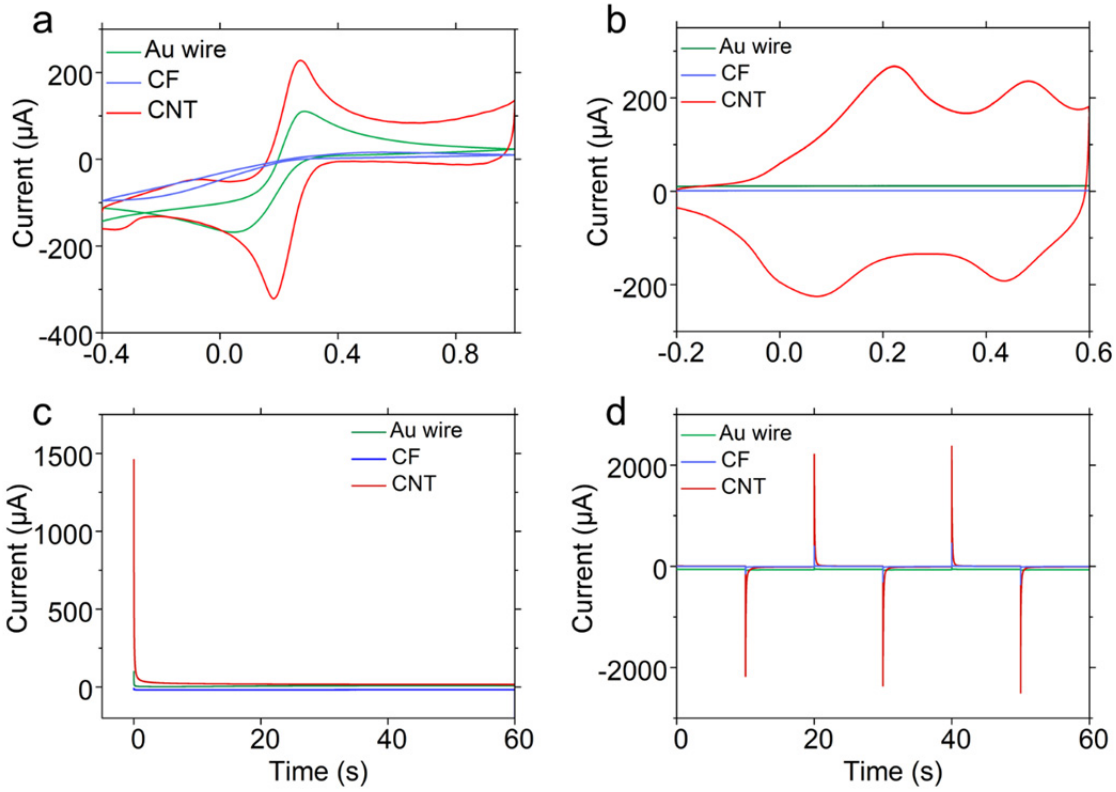

Figure S18. The electrochemical properties of CNT fibre compared with carbon fibre (CF) and gold (Au) wire (**a**–**d**, technical repeats=3)**. a**, Amperometric curves of the three electrodes in PBS (*versus* a commercial Ag/AgCl electrode). **b**, CV plots of the three fibre electrodes during the polyaniline electrodeposition process (scan rate of 100 mV/s with a commercial saturated Ag/AgCl electrode). **c**, Amperometric curves of the three fibre electrodes during the poly(3,4-ethylenedioxythiophene) electrodeposition process (initial potential of 1.25 V *versus* a commercial Ag/AgCl electrode). **d**, Amperometric curves of the electrodes during the platinum electrodeposition process.

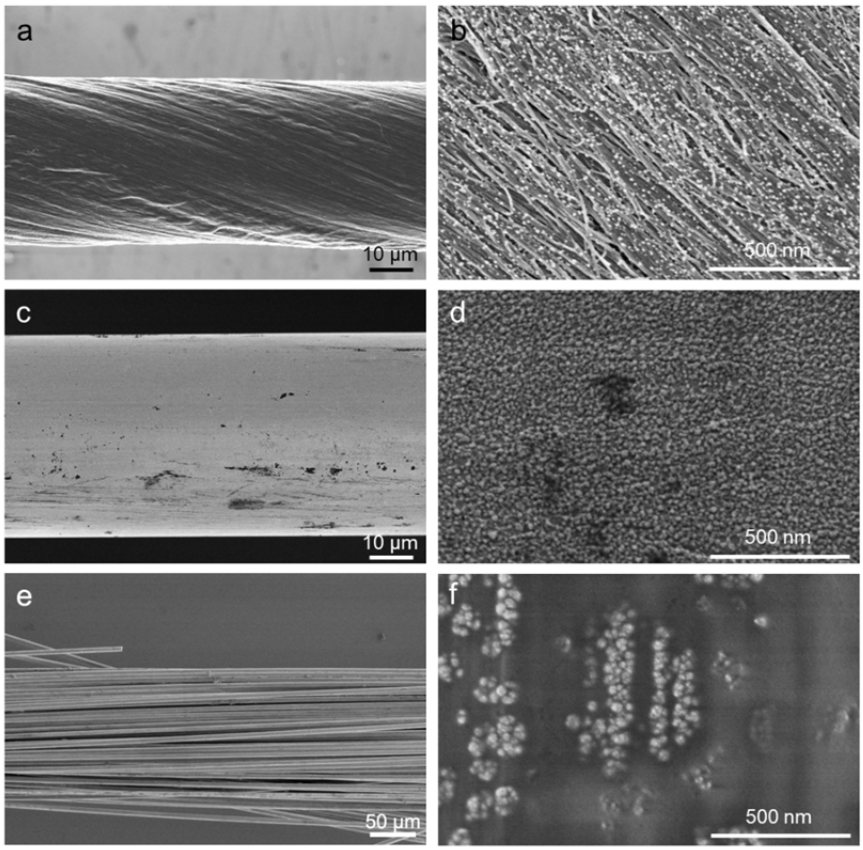

Figure S19. Representative SEM images of CNT fibre, gold wire and carbon fibre electrodeposited with platinum at low and high magnifications (technical repeats=3)**. a** and **b**, CNT fibre. **c** and **d**, Gold wire. **e** and **f**, Carbon fibre.

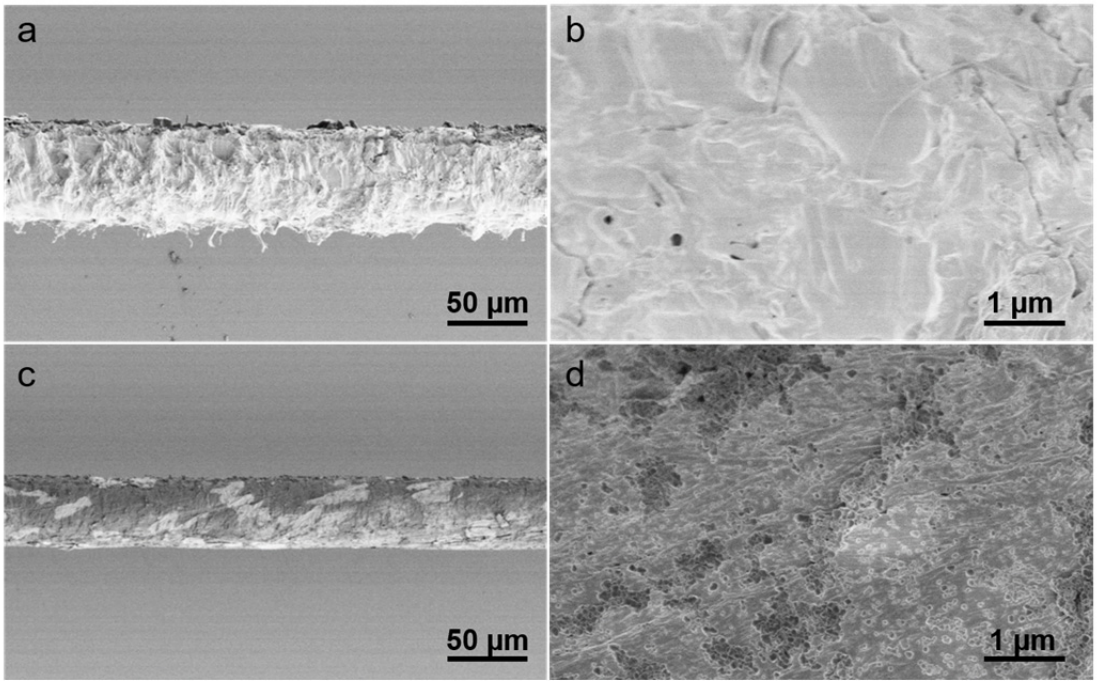

Figure S20. Representative SEM images of the Ag/AgCl reference fibre electrode (technical repeats=3). **a** and **b**, The CNT fibre electrode deposited with Ag at low and high magnifications, respectively. **c** and **d**, The Ag/AgCl reference fibre electrode at low and high magnifications, respectively.

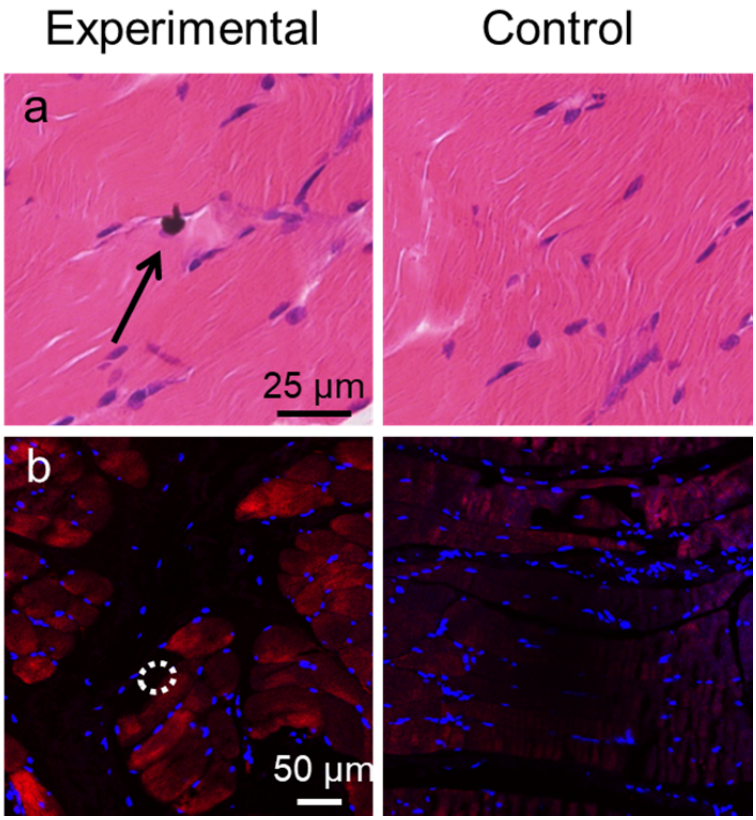

Figure S21. (**a**) Optical images of HE staining and (**b**) confocal images of CD11b staining of skeletal muscle injected with Nafion coated Ag/AgCl fibre reference electrode for 35 days (technical repeats=5). The black arrow in (**a**) and the white dotted circle in (**b**) indicate the position of fibre electrode. Blue: nucleus, DAPI; red: CD11b. The positively labelled cells are double stained by both DAPI and CD11b.

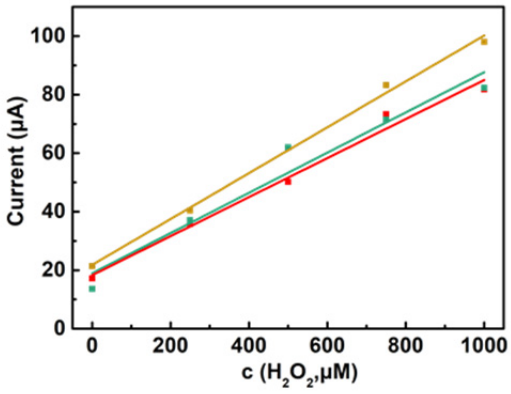

Figure S22. The reproducibility of the H_2O_2 SSFs (three samples for this sensor).

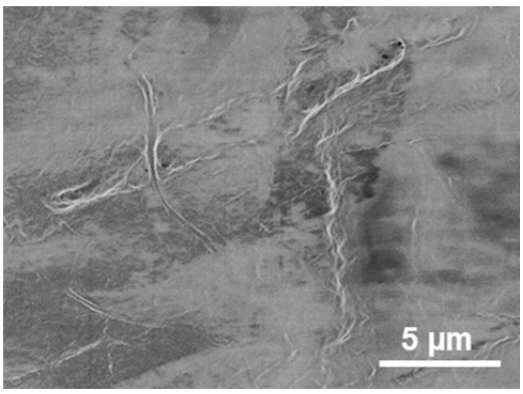

Figure S23. SEM image of the CNT fibre coated with PEDOT for Ca^{2+} SSF (technical repeats=3).

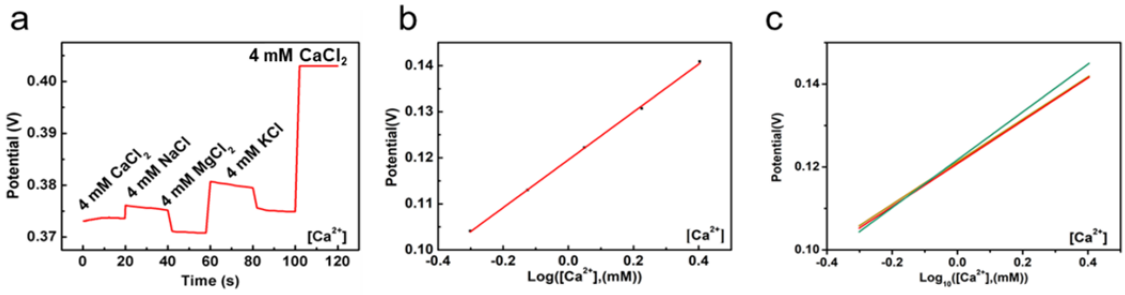

Figure S24. Basic electrochemical property of the Ca^{2+} SSF. a, The interference study of the SSF by adding different analytes showing good selectivity of the Ca^{2+} SSF (technical repeats=3). The initial concentration of solution was 4 mM and data recording was paused for 20 s for the addition of each analyte. **b**, The linear relationship between the Ca^{2+} concentration and potential of the SSF (technical repeats=3). **c**, The reproducibility of the Ca^{2+} SSFs (technical repeats=3).

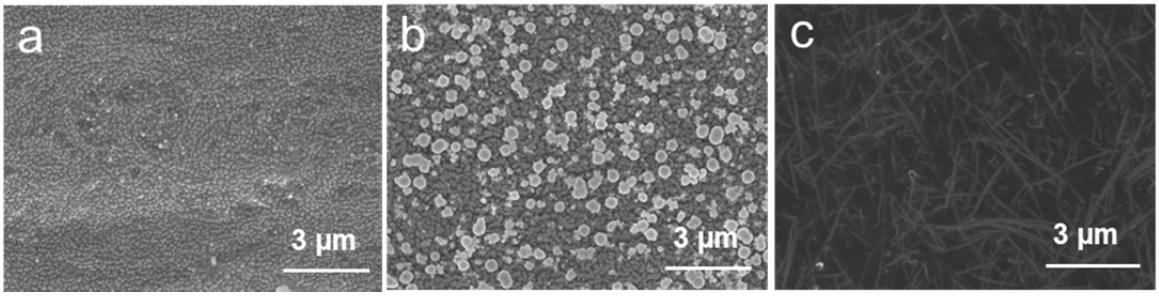

Figure S25. Representative SEM images of the CNT fibre after coating with (**a**) PANI, (**b**) PANI/Pt nanoparticles and (**c**) PANI/Pt nanoparticles/glucose oxidase for glucose SSF (technical repeats=3).

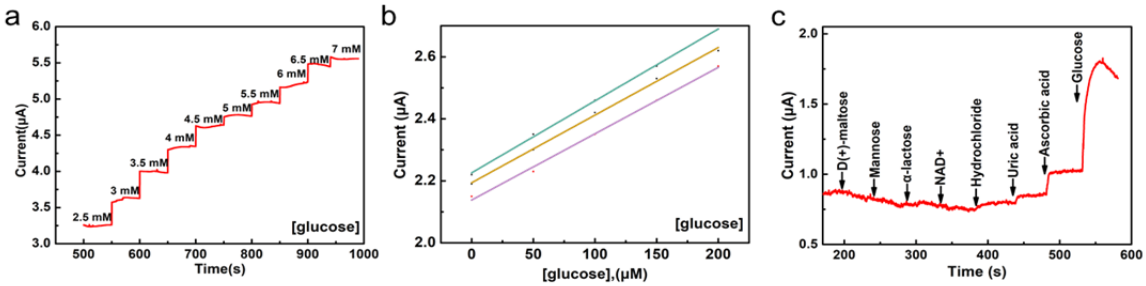

Figure S26. Characterization of the glucose SSF. **a,** The chronoamperometric responses of the SSF to the glucose/PBS solutions with increasing concentrations (technical repeats=3). The initial concentration of solution was 2.5 mM and data recording was paused for 50 s by dropping 0.5 mM glucose/PBS solution. **b**, The reproducibility of the glucose SSFs (technical repeats=3) . **c**, The interference study of the SSF by adding different analytes showing good selectivity for glucose. Data recording was paused for 50 s for the addition of each analyte (technical repeats=3).

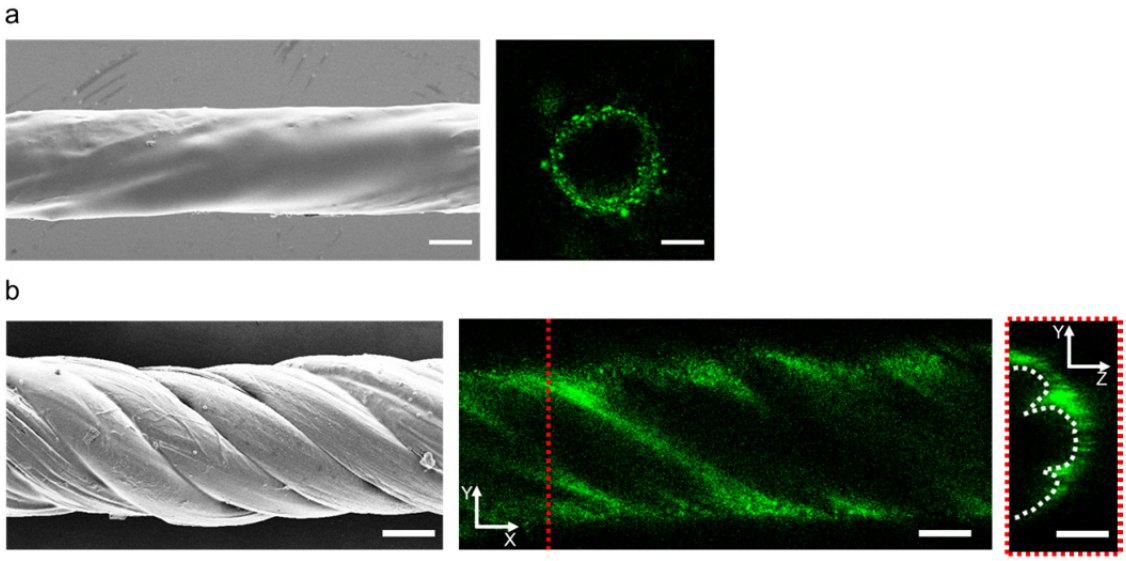

Figure S27. SEM image by side view and confocal image at cross section of the SSF (**a**) and MSF (**b**) coated with an encapsulating layer of PDMS (technical repeats=5). $SrPbBr_3$ quantum dots were incorporated into the PDMS for visualization. The thickness of PDMS was measured to be ~6 μm. Scale bar: 10 μm (**a**) and 20 μm (**b**).

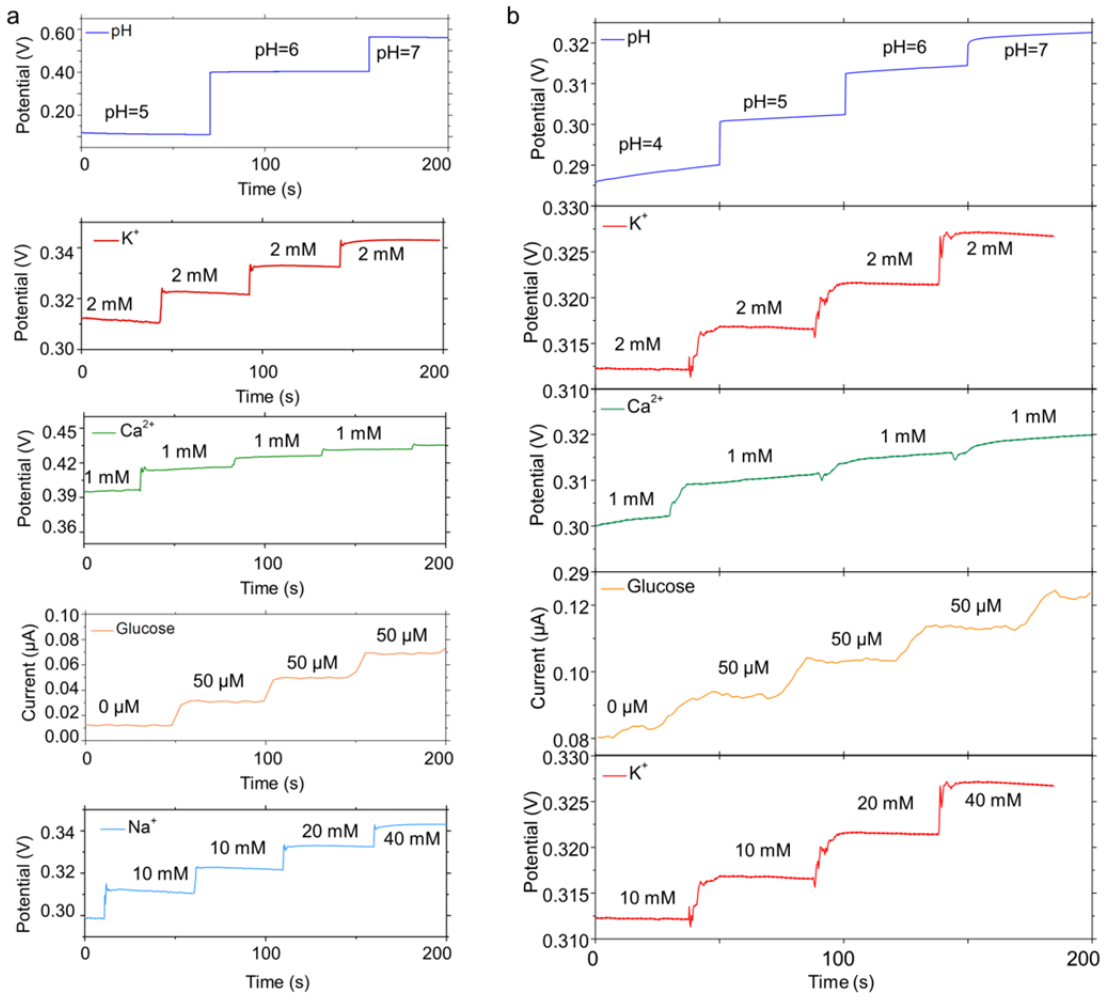

Figure S28. The sensitivity measurement of an MSF fabricated by pH, Ca^{2+}, glucose, K^+ and Na^+ SSFs (technical repeats=3)**. a**, The individual SSFs were tested respectively. **b**, The pH, Ca^{2+}, glucose, K^+ and Na^+ SSFs were assembled into an MSF and tested in a mixed solution.

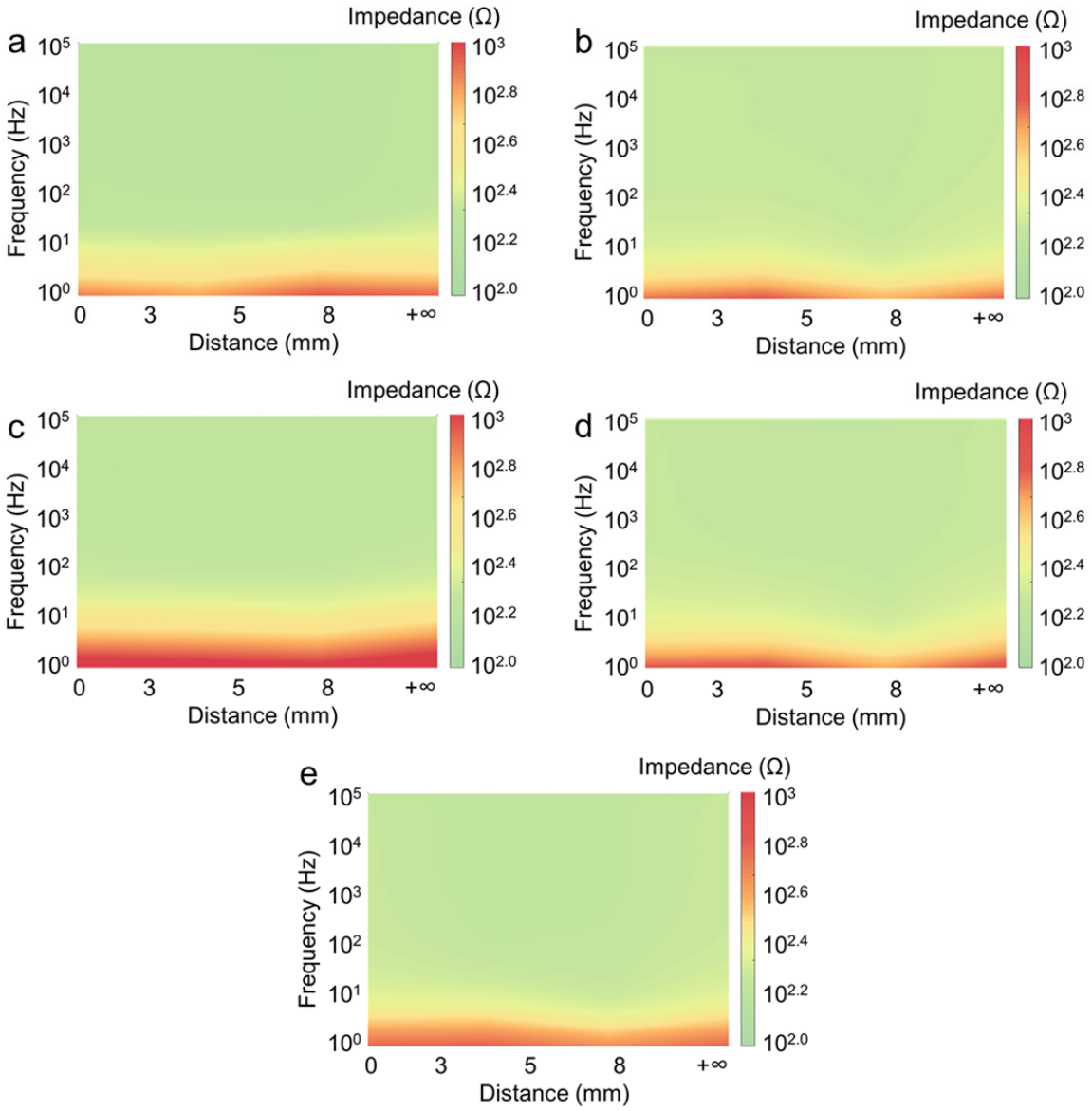

Figure S29. The impedance magnitudes of 5 H_2O_2 SSFs by changing the distance among the SSFs (0 and +∞ represent that SSFs were tested integrally and individually, respectively).

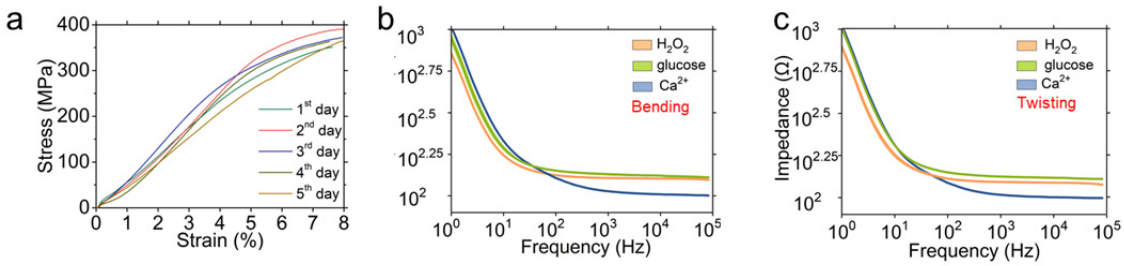

Figure S30. a, Another representative stress–strain curves of the fibres after injection into the vein of a cat for 1–5 days showing no obvious changes in tensile strength (technical repeats=3). **b** and **c**, Another representative impedance curve of every SSF in MSF under increasing frequencies after bending (**b**) and twisting (**c**) for 100 cycles showing no obvious change (technical repeats=3).

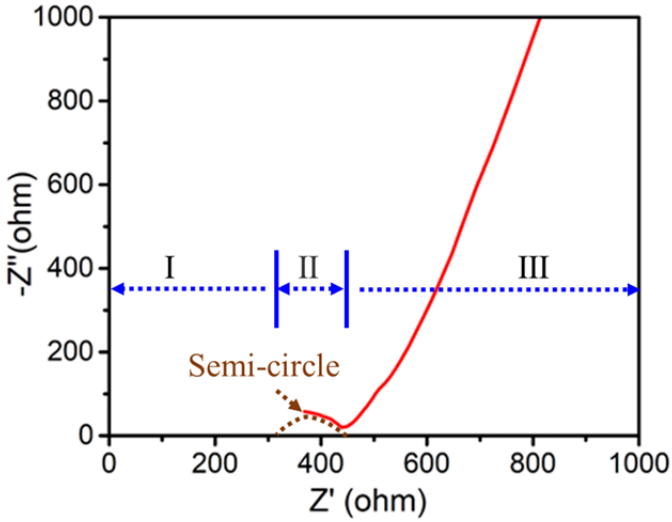

Figure S31. The Nyquist impedance diagram of SSF (technical repeats=3). The fibre sensor as the working electrode and the Ag/AgCl electrode as the reference electrode were immersed into 1×PBS solution with a frequency range of $1–10^5$ Hz. In region □ (high frequencies), the resistance measured is mainly determined by the electrode and usually composed of the following parts: the intrinsic resistance of the electrodes and the contact resistance at the interface in electrode, i.e., active material/CNT fibre. In region □ (medium frequencies), the presence of a semi-circle is observed. The diameter of this semi-circle is regarded as a pseudo-transfer resistance and is associated with the architecture of the electrode and the interface between testing environment and electrode. In region □ (low frequencies), it mainly reflects the status of the testing environment, i.e., tissues.

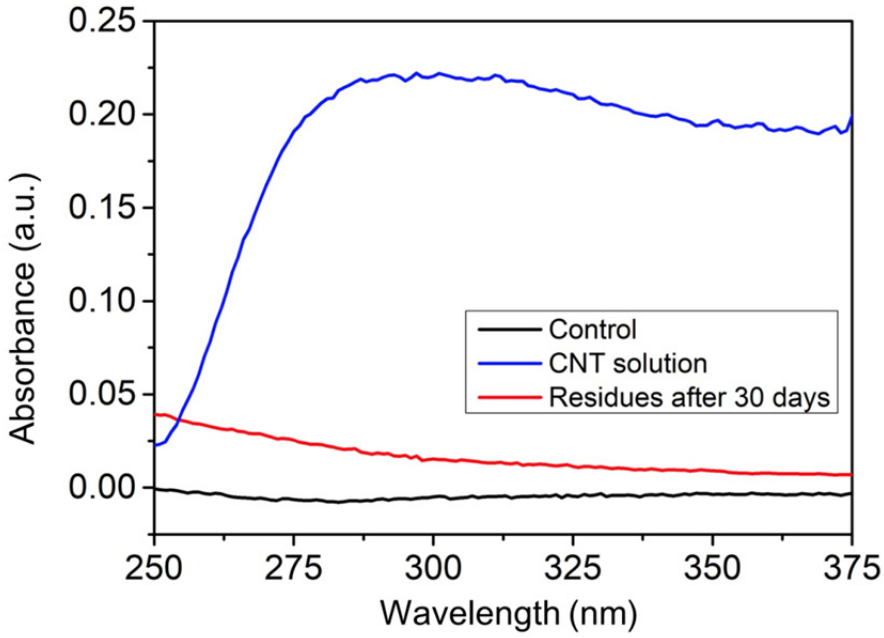

Figure S32. UV–vis spectra of as-prepared PVA/PBS solution (control), bare CNT dispersion, and residue PVA/PBS solutions after 30 days' continuous flushing of CNT fibre (technical repeats=3). No characteristic absorption peaks of CNTs were observed, indicating that they did not dissociate from the fibres.

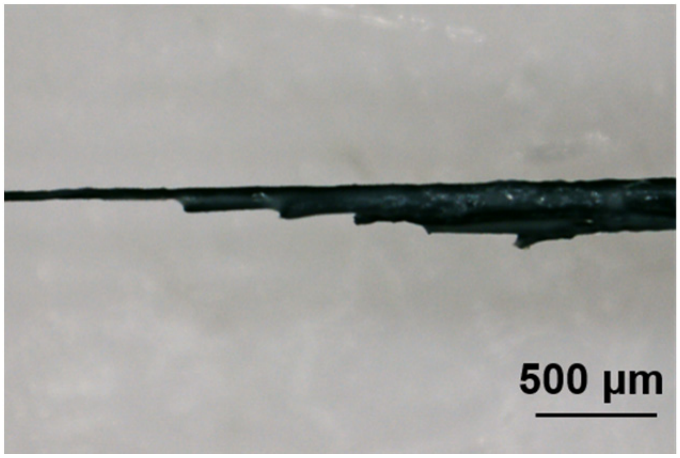

Figure S33. Representative optical image of the MSF composed of 5 H_2O_2 SSFs and reference fibre electrode with axial distributed ends (technical repeats=3).

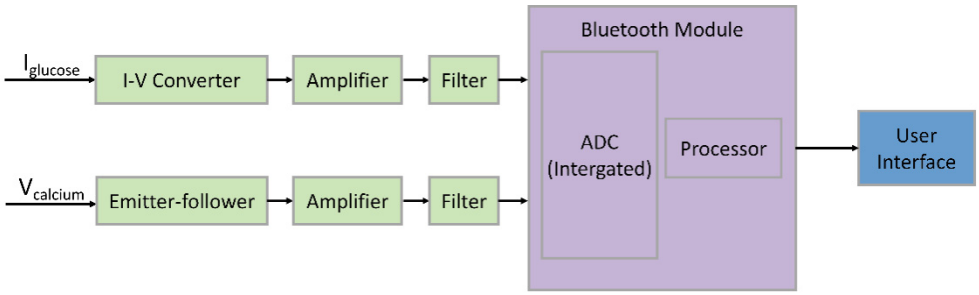

Figure S34. Block diagram of the integrated system for the MSF.

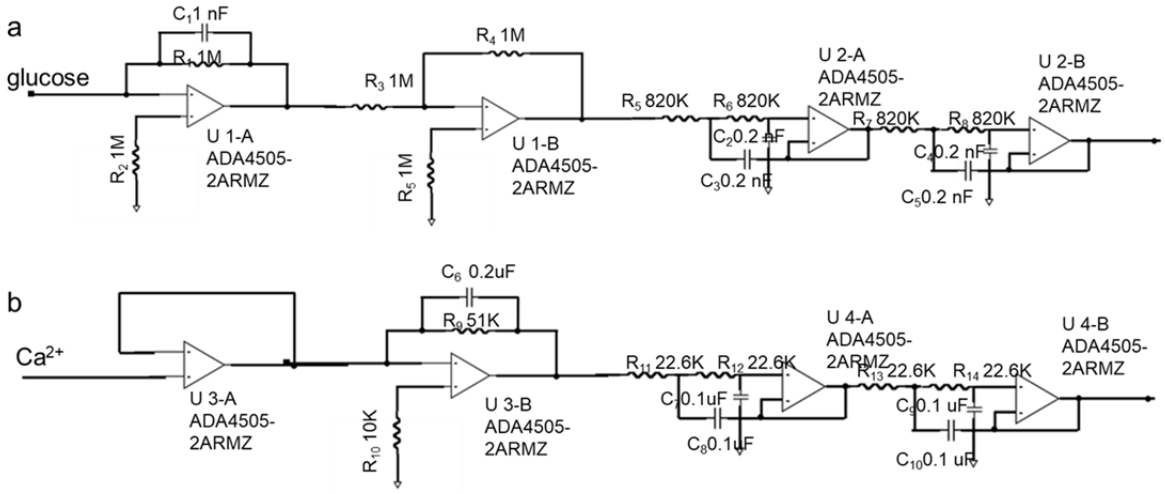

Figure S35. Schematic diagram of the integrated circuit for real-time monitoring. a, The circuit for current test. **b**, The circuit for potential test.

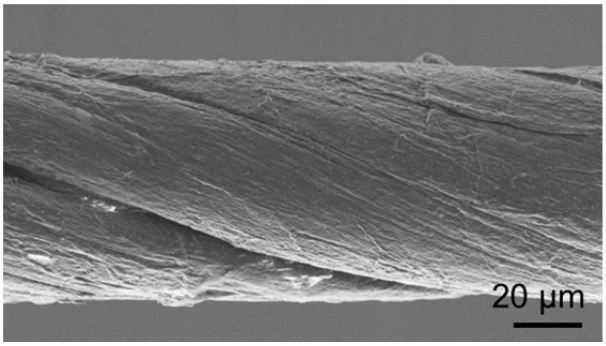

Figure S36. Representative SEM images of the Ca^{2+} SSF after implanted in the vein for 25 days (technical repeats=3).

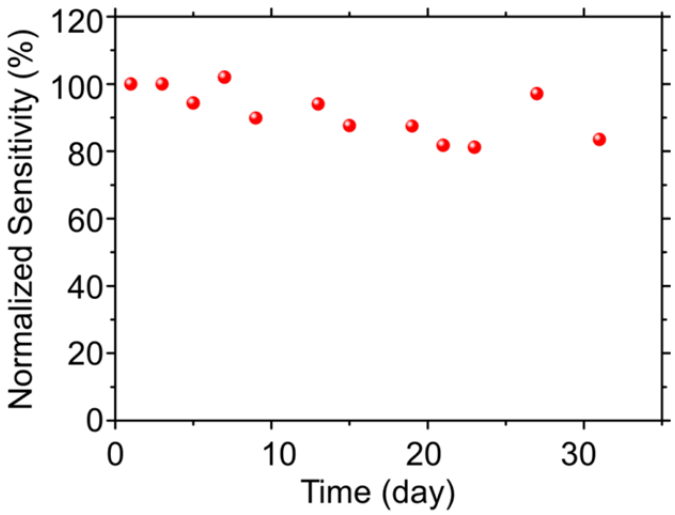

Figure S37. The sensitivity stability of ZnO-based glucose SSF *in vitro* for 31 days (technical repeats=3). The daily sensitivities of the sensor were 6.53 (1), 6.53 (3), 6.16 (5), 6.66 (7), 5.87 (9), 6.14 (13), 5.72 (15), 5.71 (19), 5.34 (21), 5.3 (23), 6.34 (27) and 5.45 (31) nA μM^{-1} (day), respectively.

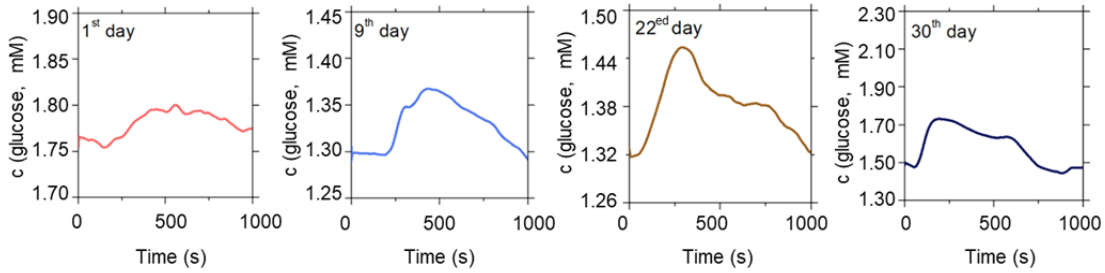

Figure S38. The test of ZnO-based glucose SSF *in vivo* for 30 days. The changes of glucose concentration in blood were introduced by the injections of 5% glucose *via* intravenous injection in the opposite leg vein of a cat.

Supplementary Movie 1

Wireless monitoring system integrated with multi-ply sensing fibres (MSF) on a living cat for real-time data transmission.

According to the different signal output of Ca^{2+} (open circuit potential) and glucose (chronoamperometric) SSFs, the corresponding circuits were designed. The whole circuit consisted of conditioning path, amplifier, filter, bluetooth module and user interface. A mobile application was designed to accompany the integrated system and to provide a user interface for data collection. After building the system, the MSF was injected into the vein of a living cat and the chip welded the whole circuit was fixed on the leg. The cat could eat and walk actively due to the safety, convenience and comfort of the wireless monitoring system. Meanwhile, the data could be transmitted to the phone (the phone interface was showed in the bottom left corner of the screen).